XI. MOLECULAR PROCESSES

There are various atomic and molecular processes that can form and destroy molecules under a variety of physical conditions. In this chapter, we will systematically review these processes, starting with the mechanisms for destroying molecules. Emphasis will be placed on two-body processes, since in most astrophysical regimes, the densities are low enough that three-body processes can be neglected.

Excellent reviews of the molecular processes that are important in interstellar clouds have been given by:

Dalgarno, A. 1975, in *Atomic and Molecular Processes in Astrophysics*, (eds. M.C.E. Huber and H. Nussbaumer).
Dalgarno, A. 1976, in *Frontier of Astrophysics*, (ed. E. Arnett).
Dalgarno, A. 1979, *Adv. Atom. Mol. Phys.* **15**, 37.
Dalgarno, A. 1987, in *Physical Processes in Interstellar Clouds*, (eds. G. Morfill and M.S. Scholer).
van Dishoeck, E.F. 1988, in *Millimeter and Submillimeter Astronomy*, (eds. R.D. Wolstencroft and W.B. Burton).

1. Photodissociation

In any astrophysical region where ultraviolet photons can penetrate, photodissociation, typically depicted as

$$ XY \;+\; h\nu \;\;\rightarrow\;\; X \;+\; Y \;\;, \tag{11.1} $$
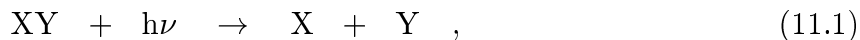
is a major destruction process of the neutral molecules. Even for molecular ions, photodissociation can be an important removal mechanism if the fraction of electrons or other negatively charged species in the region is sufficiently low. Photodissociation plays a dominant role in the chemistry of diffuse interstellar clouds and in the outer parts of dense clouds. More recently, it has been realized that cosmic ray induced photons can significantly affect the chemistry inside dense molecular clouds. Finally, photodissociation is responsible for many of the molecules and radicals observed in circumstellar envelopes, and in cometary and planetary atmospheres.

(a) Photodissociation Mechanisms

Photodissociation of a small molecule can proceed in various ways, which are illustrated in Figure 11.1 for the case of a diatomic molecule. For small polyatomic molecules, the processes are similar, but more complicated to illustrate because the potential surfaces are multi-dimensional.

The simplest dissociation process is through *direct* absorption into a repulsive upper state as shown in Figure 11.1a. This absorption may also take place into the repulsive wall of a **bound** excited electronic state (not shown). As spontaneous emission back to the ground state is relatively slow compared to the time frame for movement along the nuclear coordinate, which occurs on the picosecond time scale. All absorptions therefore lead to dissociation of the molecule. The photodissociation cross section is continuous as a function of photon energy, and its energy dependence is governed to first order by

the Franck-Condon principle in that its maximum value is at the vertical excitation energy indicated by the arrow in Figure 11.1a. This is the predominant photodissociation pathway of astrophysically important molecules such as CH^+, NH, HCl, CH_4, ...

In contrast to direct photodissociation, which involves continuous absorption and can therefore occur over a range of wavelengths, the *indirect* photodissociation mechanisms each involve discrete transitions to bound vibrational levels of an excited electronic state as a first step. This has profound implications for the transfer of radiation, because line absorption can be saturated much more readily than continuous absorption. In the case of *predissociation*, illustrated in Figure 11.1b, the bound levels of the excited electronic state are coupled to the vibrational continuum of a third state of different symmetry. The third state usually crosses the excited electronic state within the adiabatic Born-Oppenheimer approximation. The transition to the dissociating state occurs without the emission of radiation, and can in most cases be described by first order perturbation theory. This mechanism is thought to be the predominant way of photodissociating CO. The spectral signature of this process appears as a broadening of the discrete peaks (corresponding to absorption into the bound excited state), due to the interaction with the third state.

In the process of *coupled states photodissociation*, illustrated in Figure 11.1c, the bound levels of the excited state couple with the continuum of a dissociative state of the same symmetry which, in the Born-Oppenheimer approximation, does not cross the bound state. If the states have a close "avoided-crossing", the interaction is strong, and requires a coupled states description of the process. The spectral features in this case vary depending on the strength of the coupling and the relative sizes of the transition dipole moments involved. For example, they may consist of a broad continuous absorption background on which is superposed a series of sharper resonances. This mechanism appears to play an important role in the photodissociation of CH and OH in interstellar clouds.

Finally, in the process of *spontaneous radiative dissociation*, illustrated in Figure 11.1d, the bound excited states simply decay by spontaneous emission into the vibrational continuum of either the ground electronic state, or a lower-lying repulsive state. The absorption cross section consists in this case of a series os sharp, discrete peaks. The photodissociation of H_2 takes place through this mechanism.

All of these processes may contribute to the photodissociation of a particular molecule, although in some cases one specific process may dominate. Let us look at some examples of diatomic molecule photodissociation in more detail.

(ii) Direct Photodissociation

The clearest example of a molecule for which direct photodissociation dominates is provided by the $H_2{}^+$ ion, for which the potential energy curves are reproduced in Figure 11.2 (see also Figure 7.1). In interstellar environments, the molecule is almost entirely in the lowest vibrational and rotational level. Photodissociation can occur by direct absorption into the repulsive 2p σ_u state. The continuum vibrational wave function is also illustrated in Figure 11.2.

The cross section for photodissociation at a photon energy $E = \Delta E_{k'v''}$ is given by the formula

$$\sigma(E) = \frac{2}{3}\frac{\pi e^2}{m_e c}g\Delta E_{k'v''}|<k'|D^{el}(R)|v''>|^2 \quad , \tag{11.2}$$
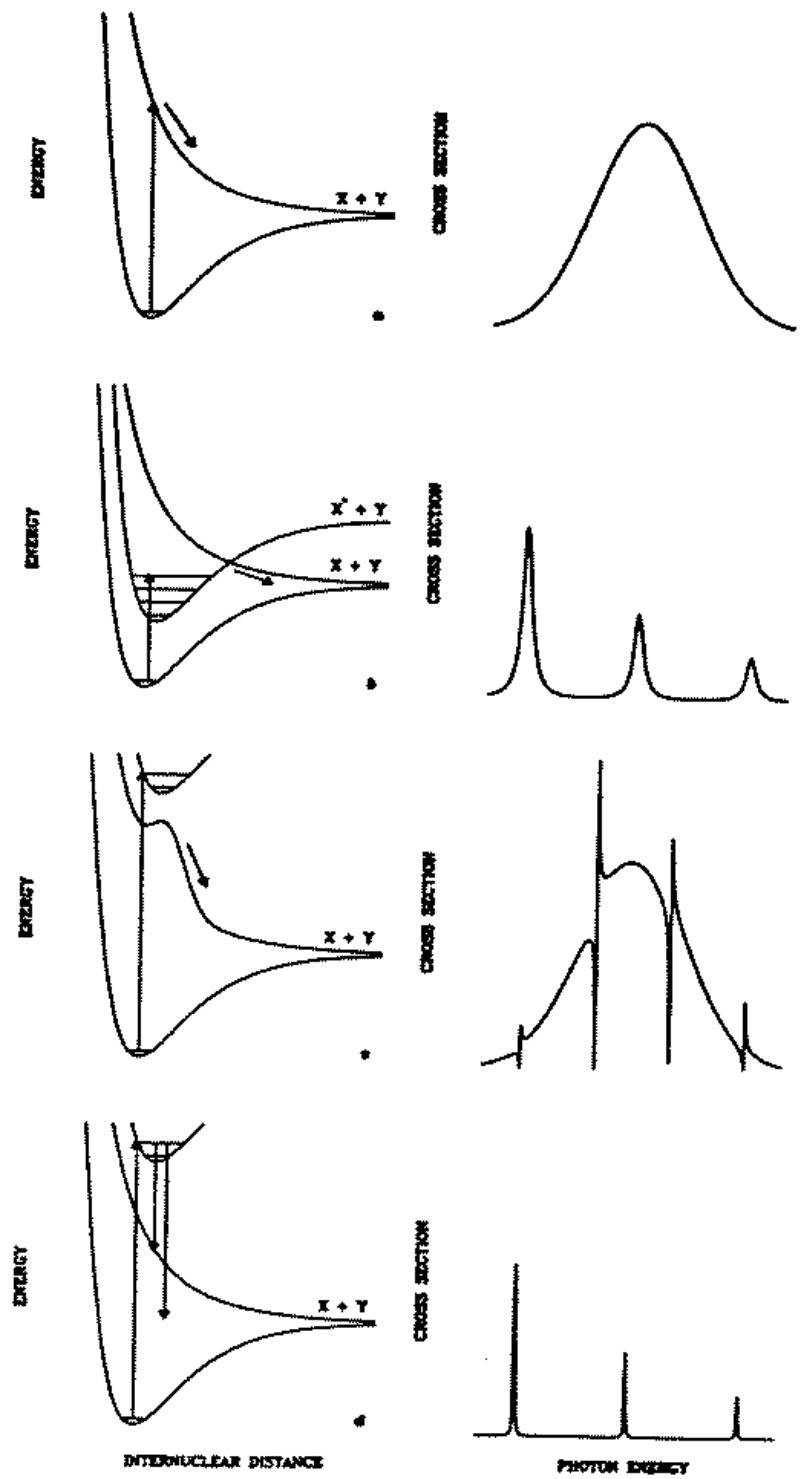
Figure 11.1– Potential energy curves and characteristic cross sections for the processes of (a) direct photodissociation; (b) predissociation; (c) coupled states photodissociation; (d) spontaneous radiative dissociation.
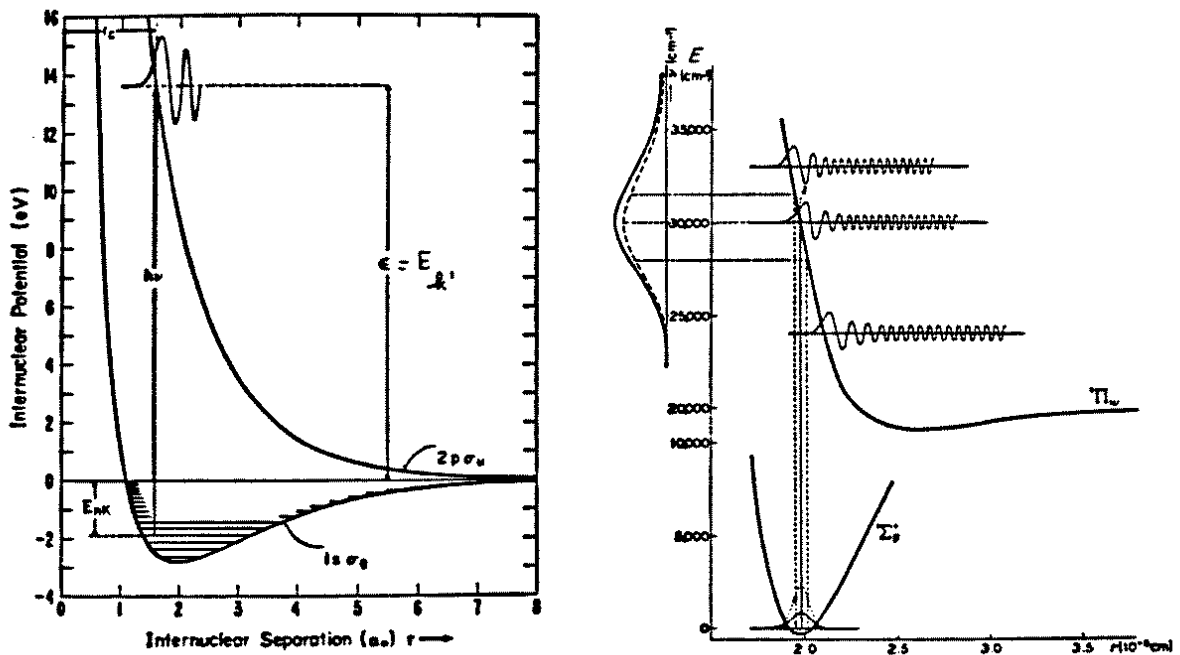
Figure 11.2– Potential energy curves for H_2^+ (left). Right: The reflection principle.
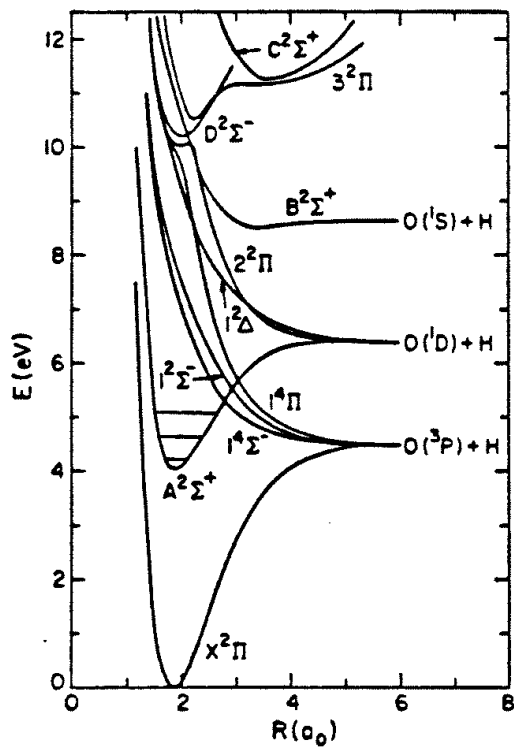

Figure 11.3– Potential energy curves for the OH molecule.

which is very similar to the formula for the oscillator strength for a bound-bound transition. The wavenumber k' corresponds to the energy $E_{k'} = \Delta E_{k'v''}$ - $(E_f(R \rightarrow \infty)$ - $E_{v''})$ of the nuclei above the dissociation limit. If both the matrix element and the transition energy $\Delta E_{k'v''}$ are in atomic units, the factor $2\pi e^2/3m_e c$ has the numerical value 2.69 $\times$ 10^{-16} cm^{-2}. Figure 11.2 (right) illustrates that the cross section reflects the shape of the vibrational wavefunction in the lower state. The maximum usually occurs close to the vertical excitation energy. Note that the cross section is often negligibly small at the threshold wavelength, corresponding to the dissociation energy of the molecule. Thus, the dissociation energy of a molecule is *not* a good measure of how rapid a molecule is photodissociated; this depends entirely on the availability of excited electronic states through which photodissociation can occur by one of the four processes discussed above. For example, the dissociation energy of H_3^+ is only ~5 eV, but the photodissociation of interstellar H_3^+ is negligible since its first excited state occurs at 18 eV.

A molecule with a more complicated electronic structure such as OH generally has several low-lying photodissociation channels, as illustrated in Figure 11.3. In this case, direct photodissociation can occur by absorption into, for example, the 1 $^2\Sigma^-$, 1 $^2\Delta$, and B $^2\Sigma^+$ states.

A well-known example of a molecule for which direct photodissociation can occur by direct absorption into the repulsive part of a potential curve which exhibits a bound well at larger distances, is provided by the O_2 molecule. As shown in Figure 10.4 and 10.5, absorption into the $B^3\Sigma_u^-$ - $X^3\Sigma_g^-$ Schumann-Runge continuum will lead to photodissociation of the molecule. In this case, the relative amounts of discrete and continuous absorption are very sensitive to small uncertainties in the relative positions of the upper and lower potential curves. An instructive example, illustrated in Figure 11.4, is provided by the photodissociation of the isovalent CH^+ and SiH^+ ions through the $A^1\Pi$ state. For CH^+, nearly 100% of the absorption cross section occurs into discrete levels. For SiH^+, however, the curves are slightly displaced, and most of the absorption takes place into the continuum of the A state. Thus, the photodissociation of SiH^+ through the A state will be very rapid, whereas for CH^+ it will be negligible.

In many texts, the reflection approximation is presented as shown in Figure 11.2. However, this version is, rigorously, incorrect. The Franck-Condon approximation in fact states that *both* the position **and** momentum of the nuclei are conserved during the electronic transition. For low-lying states such as that shown in Figure 11.2, the amount of potential (or kinetic) energy is small, and so the reflection approximation is often invoked with arrows emanating at the energy level of the initial state and terminating on the repulsive potential. In Figure 11.5, the more correct treatment is outlined, in this case for emission from a bound upper state to a repulsive lower state. If V_e and V_g are the excited and ground state potentials, and $T(R)$ is the kinetic energy of the nuclei, the *Mulliken difference potential* is defined as $V_{Mulliken} = V_g(R) + T(R)$. The nature of the Mulliken difference potential is illustrated in Figure 11.5 for a series of repulsive potentials that range from very steep to very flat. The turning points remain the same, but clearly there can be major differences in regions where there are considerable amounts of kinetic energy. The wavelength of emission (or absorption) is given by

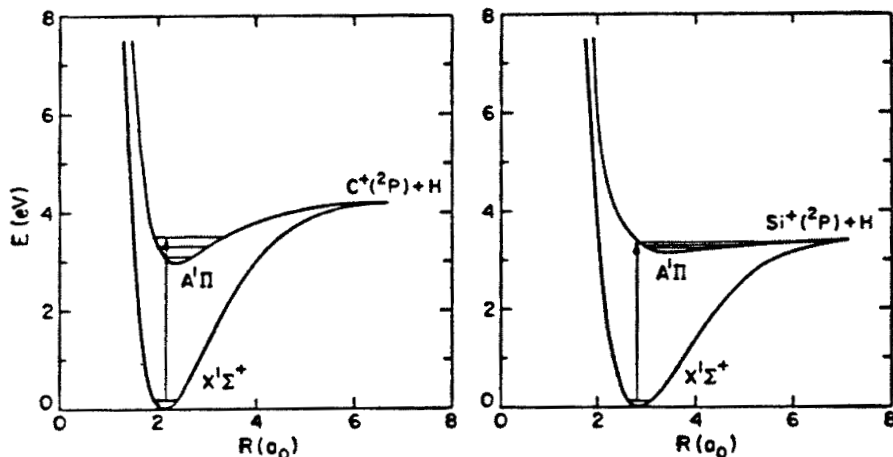$$h\nu \quad = \quad E - [V_g(R) + T(R)] \quad = \quad V_e(R) - V_g(R) \quad ,$$

Figure 11.4– Comparison of the photodissociation of CH^+ and SiH^+ via the $A^1\Pi$ state.

and so we see the correct reflection approximation either must draw arrows from the bound state energy level to the Mulliken difference potential, or from the initial potential energy curve to the final potential energy curve. In either case, the turning points define the (approximate) limits.

As Figure 11.5 shows, when the repulsive potential is fairly flat and/or the vibrational energy content of the bound state is high, the difference potential goes through a maximum. This maximum creates the possibility for emission at one frequency at *two* internuclear distances, and results in interference. The net result is oscillatory behavior in the emission or absorption. In Figure 11.5, the narrow, or fast, oscillations arise from the structure in the upper and lower state wavefunction, that it is arises from the nodal character of the vibrational state wavefunctions. Thus, the top plots in Figure 11.5 look very much like vibrational wavefunctions at high v. As the Mulliken difference potential becomes more important, *broad* oscillations are superposed on the nodal nature of the vibrational wavefunctions, as is illustrated by the dotted profiles in the lower sections of Figure 11.5. The overall result is a very complex emission (or absorption) spectrum, particularly for high vibrational bands which have a great deal of kinetic energy and lots of nodal structure in their wavefunctions.

(ii) Predissociation

In addition to the direct photodissociation channel, the OH molecule also has predissociation channels. For example, the bound $A^2\Sigma^+$ state is crossed by the repulsive $1^4\Sigma^-$, $1^2\Sigma^-$, and $1^4\Pi$ states (see Figure 11.3), which leads to rapid predissociation of all vibrational levels of the A state with $\nu \geq 2$. The strength of the predissociation process can be described by first-order perturbation theory. The rate for predissociation of level i, v', J' by a final electronic state f, k, J is then given by the **Fermi-Wentzel Golden Rule** formula

$$k^{pr}_{\nu' J'} \quad = \quad \frac{2\pi}{h} | < iv'J' | H_{int} | fkJ > |^2 \qquad \text{s}^{-1}, \tag{11.3}$$
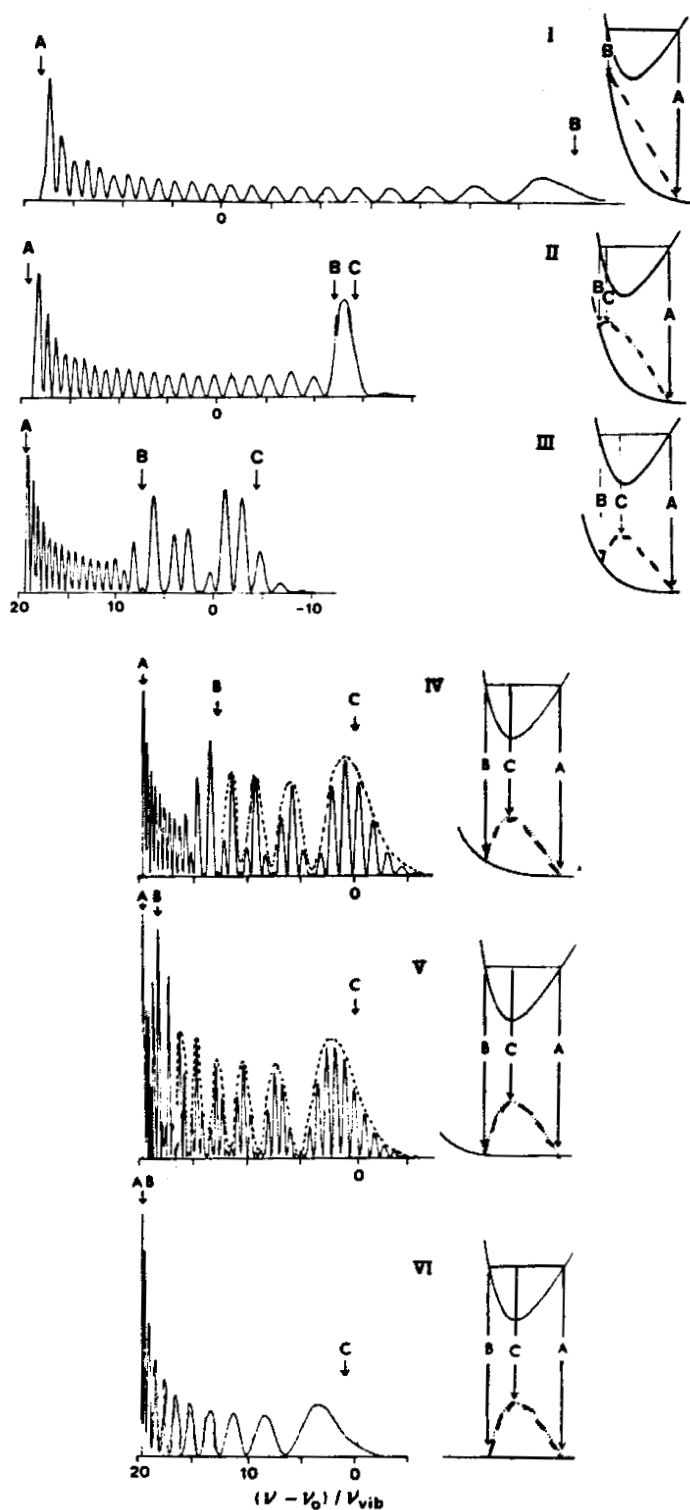
Figure 11.5– An illustration of the "correct" reflection approximation. Shown are the Franck-Condon factors and wavefunctions for an emission from a bound state with considerable vibrational excitation onto a purely repulsive lower state potential. The dotted curves on the lower states are the Mulliken difference potential, and a variety of repulsive curves – from very steep to very shallow – are shown. The arrows labeled A, B, and C indicate the transitions from positions which correspond to the classical turning points and the maximum of the Mulliken difference potential.

where H_{int} stands for the interaction Hamiltonian, which may, for example, be the spin-orbit interaction.

Another very important astrophysical example is the CO molecule. CO is a very stable molecule with a dissociation energy of 11.09 eV, so that the threshold for photodissociation lies at 1118 Å. The interstellar radiation field only has photons with wavelengths $\lambda > 912$ Å (see below), so that photodissociation of interstellar CO can occur only in the region 912 Å$< \lambda < 1118$ Å. Laboratory experiments show that the molecule has no continuous absorption in this energy range (see Figure 11.6), so that the photodissociation must occur by absorption into predissociating states, such as the $C^1\Sigma^+$ and $E^1\Pi$ states, and higher-lying states. Because the photodissociation occurs by line rather than by continuous absorption, this has profound astrophysical consequences for the radiative transfer, which needs to be discussed in some detail.

In the case of direct photodissociation, the cross section is continuous as a function of photon energy, and is typically 10^{-18} cm^2, so the optical depth for absorption presented by a slab of molecules of column density N in the initial state is

$$\tau = N\sigma \sim 10^{-18}N \ . \tag{11.4}$$

For comparison, consider a UV transition of a molecule with $\tilde{\nu} = 10^5$ cm^{-1} or $\lambda = 1000$ Å, and a fairly large oscillator strength, $f \sim 0.1$. The peak absorption cross section at line center in this case is

$$\sigma \sim \frac{\int \sigma d\nu}{\Delta \nu} \ . \tag{11.5}$$

From the oscillator strength sum rule, $\int \sigma d\nu = (\pi e^2/m_e c)f$. In a cold interstellar cloud, for example, the line width may be as small as that for thermal Doppler broadening at T = 100 K, i.e.

$$\frac{\Delta v}{c} \sim \frac{1}{3 \text{ x } 10^5} \sim \frac{\Delta \nu}{\nu} \ , \tag{11.6}$$

so that

$$\sigma \sim \frac{0.02654 \text{ x } 0.1}{10^5 c/3 \text{ x } 10^5} \sim 3 \text{ x } 10^{-13} \quad \text{cm}^2, \tag{11.7}$$

which is orders of magnitude larger than a typical continuous cross section, although effective over only a narrow frequency interval. As a consequence, line absorption will become optically thick or saturated (i.e. $\tau > 1$) more readily than will continuous absorption. When this occurs, the absorption rate drops drastically with increasing depth into the absorbing slab because "all" of the photons have already been absorbed. If the slab is sufficiently thick, the molecules near the surface can thus effectively **shield** the molecules at greater optical depths from the dissociating photons.

The abundance of CO in interstellar clouds is sufficiently high that the predissociating lines readily become self-shielding, thus enhancing the CO concentration even more. Line absorptions also lead to isotope-selective processes, which will be discussed below.

(iii) Coupled-States Photodissociation

An example of a molecule for which the coupled states process is important is again the OH molecule. As Figure 11.3 shows, the $2^2\Pi$ and $3^2\Pi$ states undergo a so-called
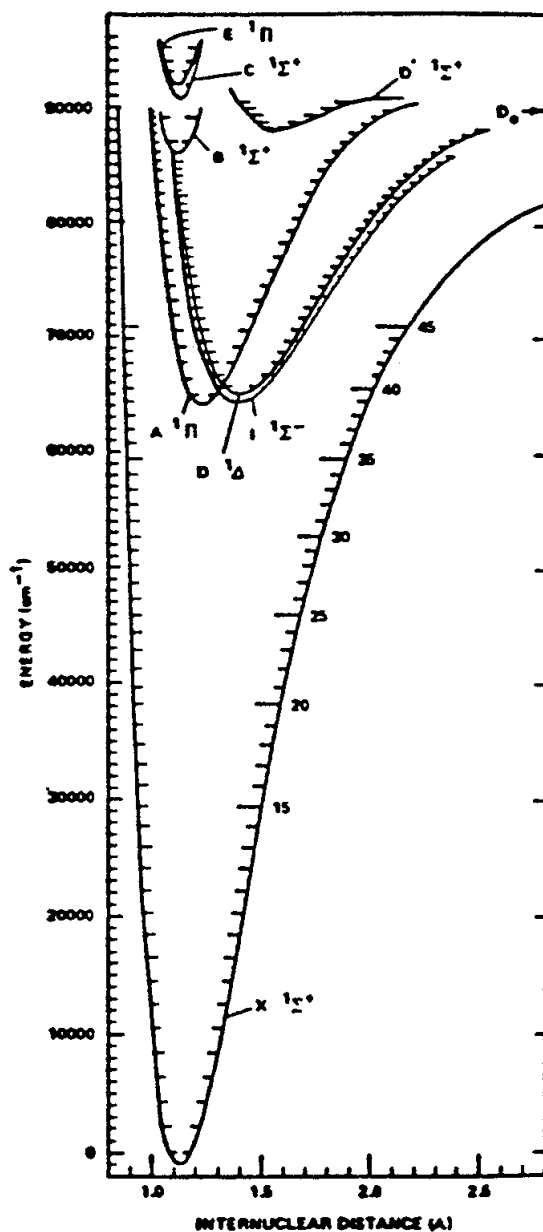
Figure 11.6– Potential energy curves for the CO molecule.

avoided crossing in the neighborhood of R_{eq}. The resulting cross section for absorption is similar to that illustrated in Figure 11.1c. Since it is mostly continuous, no self-shielding occurs.

(iv) Spontaneous Radiative Dissociation

For most molecules, this photodissociation mechanism plays only a minor role, but it is the dominant photodissociation process of the most important astrophysical molecule, H_2. Figure 11.7 illustrates the potential energy curves involved. In the first step of the process, an H_2 molecule in the $\nu = 0$ vibrational level of the ground $X^1\Sigma^+$ electronic

– 262 –

state absorbs an ultraviolet photon into an excited electronic state. For photon energies less than 13.6 eV, only the $B^1\Sigma_u^+$ and $C^1\Pi_u$ states can be accessed through electric dipole allowed transitions. The corresponding series of discrete absorptions into the various levels are called the **Lyman** and **Werner** systems, respectively. The electronically excited levels decay rapidly by spontaneous emission into the vibrational continuum of the ground state, leading to dissociation of the molecule. Detailed calculations of the radiative transition probabilities for this process show that on the average, 10% of the absorptions lead to dissociation in the interstellar radiation field.

The remaining 90% of the fluorescent transitions populate various bound excited vibration-rotation levels of the ground $X^1\Sigma^+$ state. These levels subsequently decay through slow quadrupole transitions at infrared wavelengths, giving rise to spectra such as those shown in Figure 9.3. H_2 ultraviolet emission lines resulting from electron-impact excitation, rather than photon excitation, have been observed in the Jovian atmosphere (Yung *et al.* 1982, *Ap. J.* **254**, L69). They can also be seen in the UV spectrum shown in Figure 6.34.

The main reason for the large abundance of H_2 in interstellar clouds is the fact that its photodissociation is initiated by line absorptions. These lines are not broadened due to any predissociation mechanism, but only due to the finite radiative lifetime of the state, so that they are very narrow. Thus, the lines rapidly become optically thick, and the H_2 molecule also shields itself quite effectively.
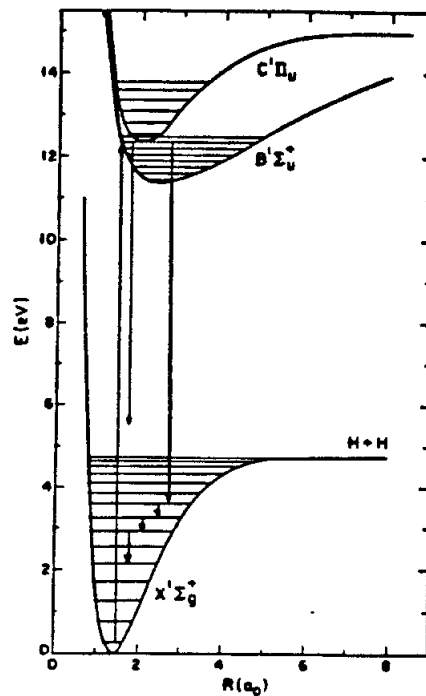

Figure 11.7– Potential energy curves illustrating the photodissociation and excitation processes of H_2.

(b) Photodissociation Cross Sections

How do we obtain photodissociation cross sections?

(i) Theory

Ab initio quantum chemical calculations can provide potential energy curves and transition dipole moments connecting the excited states with the ground electronic state. For direct photodissociation, the eigenvalues for the nuclear motion (7.35) can then be solved by numerical integration, and cross sections can be obtained through eq. (11.2). For indirect processes, oscillator strengths and predissociation rates can be computed according to eq. (11.3). The *predissociation probability* is then obtained by comparing k^{pr} with the inverse radiative lifetime of the molecule A^{rad}:

$$n_u \quad = \quad k^{pr}/(k^{pr} + A^{rad}) \ .$$ (11.8)

If the coupling is strong, as often occurs for the case illustrated in Figure 11.1c, perturbation theory is no longer valid, and the coupled equations have to be solved. Theory can provide transition energies accurate to better than about 0.3 eV and cross sections to better than 30% for small molecules, with the number of electrons less than about 30. In practice, reliable calculations are also limited to the lowest 4-5 electronic states per molecular symmetry. For most molecules of astrophysical interest, this range includes the dominant photodissociation channels. An important exception is, e.g., CO.

(ii) Experiment

The information obtained from experiment is often complementary to that observed from theory. Laboratory measurements of absorption cross sections have been performed for chemically stable species such as H_2O, CO_2, NH_3, CH_4, etc... Most of these experiments are performed at rather low resolution at national or international synchrotron facilities, where the individual rotational lines are not resolved. Typical examples of measured cross sections are reproduced in Figure 11.8. For CH_4, various absorption continua are observed, with discrete features superposed at shorter wavelengths. The absorption of NO occurs mostly in discrete bands. Note that often the electronic states responsible for the absorptions have not been identified spectroscopically. Recently discovered non-linear mixing techniques promise to push very high resolution laser-based photodissociation experiments well into the vacuum-ultraviolet.
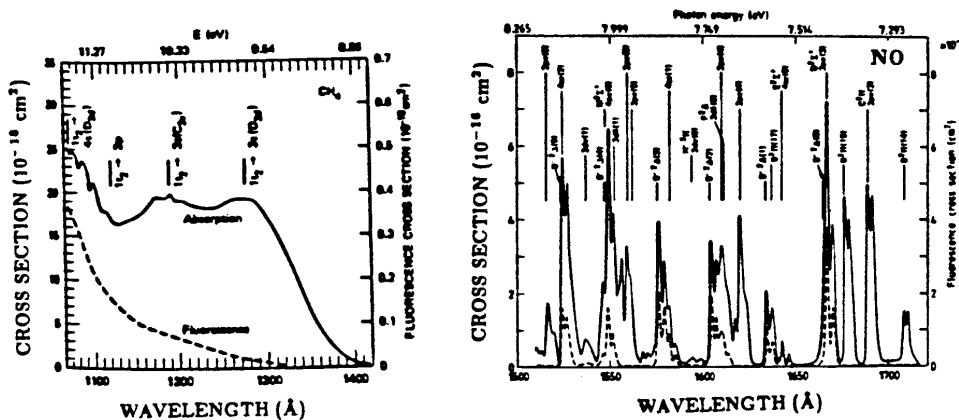

Figure 11.8– Measured absorption (full lines) and fluorescence (dashed lines) cross sections for CH_4 (*left*) and NO (*right*).

The absorption of a photon can result in re-emission of another photon (fluorescence), dissociation, or ionization of the molecule, and many experiments do not distinguish between these processes. If the photon energy is insufficient to ionize the molecule and if the absorption is continuous, it is likely that photodissociation is the dominant process. In other cases, additional information on the fluorescence and/or ionization cross sections is needed to infer the dissociation probabilities n_u. For some species, the fluorescence cross sections have been measured explicitly. Figure 11.8b compares the absorption and fluorescence results for NO. It appears that for some bands the fluorescence yield is large; whereas for other bands photodissociation occurs with near 100% probability. The absorption cross sections for continuous processes measured at low resolution are quite accurate. However, for discrete absorptions, high spectral resolution and low pressures are essential to obtain reliable experimental results, because saturation effects can easily cause orders of magnitude errors. Another experimental problem arises from the lack of powerful continuous light sources at vacuum ultraviolet (VUV) wavelengths $\lambda \lesssim 1100$ Å to date. As noted above, measurements using synchrotron radiation are possible, but only very few facilities have spectrographs with sufficiently high resolution. Some beautiful experiments have been performed with VUV lasers, and more can be expected. Nevertheless, it is only for a few stable molecules that reliable cross sections are available at the shortest wavelengths. Experimental data on reactive molecules, such as the radicals CH, OH, C_2H, ... are still extremely limited.

(c) Photodissociation Rates

The rate of photodissociation of a molecule by absorption from a lower level l into a continuous upper channel u is given by

$$k_{pd}^{cont} \quad = \quad \int \sigma_{ul}(\lambda)x_l J(\lambda)d\lambda \qquad [\text{s}^{-1}], \tag{11.9}$$

where x_l is the fractional population in level l, and $J(\lambda)$ is the mean intensity of the radiation measured in ph cm^{-2} s^{-1} Å^{-1}. For indirect processes, the rate of dissociation by absorption into a specific level of a bound upper state u from the lower level l is

$$k_{pd}^{line} \quad = \quad \frac{\pi e^2}{m_e c^2}\lambda_{ul}^2 f_{ul} n_u x_l J(\lambda_{ul}) \qquad [\text{s}^{-1}]. \tag{11.10}$$

The numerical value of $\pi e^2/m_e c^2$ is 8.85 x 10^{-21} in the adopted units. The total photodissociation rate of a molecule is obtained by summation over all possible channels. The effectiveness of each channel depends on the characteristics of the radiation source. Photodissociation channels with large cross section but at energies of low photon flux maybe less significant than channels with smaller cross sections at the peak of the photon flux.

(d) Radiation Fields

(i) Background Interstellar Radiation Field

The ensemble of bright, young stars in the Galaxy give rise to a background interstellar radiation field. Estimates of the strength of this radiation in the solar neighborhood have
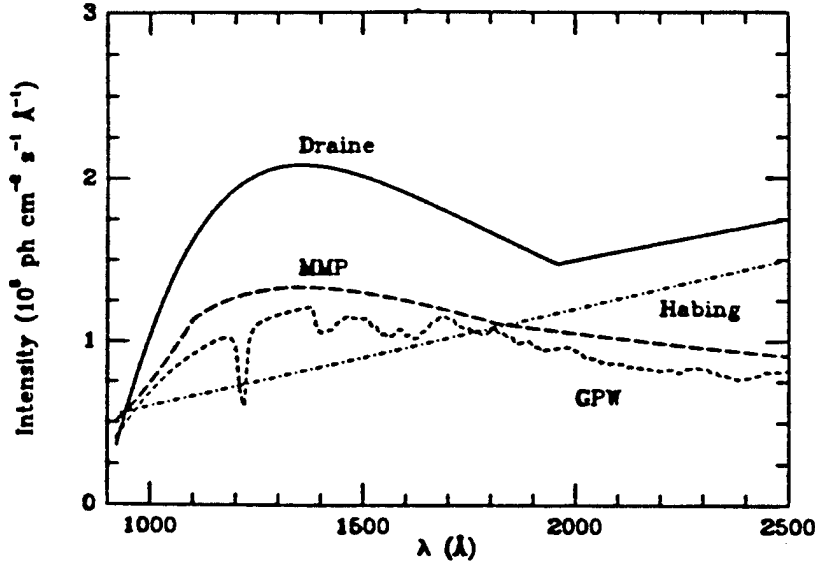
Figure 11.9– The intensity of the interstellar radiation field as a function of wavelength. From van Dishoeck (1988).
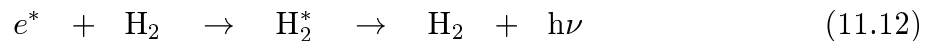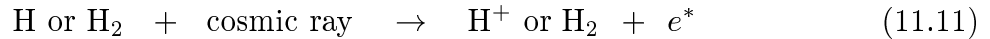
been made by various people, and are summarized in Figure 11.9. The intensities vanish below 912 Å (13.6 eV) due to absorption by atomic hydrogen in the vicinity of the stars where the photons originate. Note that few direct measurements exist at $\lambda <$ 1100 Å, the important wavelength region for H_2 and CO photodissociation and C photoionization.

(ii) Lyman-α Radiation

In interstellar regions subjected to fast shocks, the radiation field may have a very high intensity at 1215.6 Å, because of recombination and collisional excitation of atomic hydrogen leading to Lyman-α radiation. It is thus important to know whether a molecule has a photodissociation channel at this wavelength. Molecules such as H_2, CO, and N_2 cannot be destroyed by Lyman-α radiation, whereas other species like OH and H_2O have cross sections of a few times 10^{-18} cm^2 at 1215.6 Å and are thus easily destroyed.

(iii) Cosmic-Ray Induced Photons

Most models of interstellar clouds assume that the ultraviolet photons of the background radiation field cannot penetrate the inner parts of dense clouds. However, a dilute flux of ultraviolet photons can be produced following excitation of H_2 by energetic secondary electrons resulting from cosmic ray ionization of H and H_2:

$$\text{H or } H_2 \;+\; \text{cosmic ray} \;\;\rightarrow\;\; H^+ \text{ or } H_2 \;+\; e^* \qquad (11.11)$$

$$e^* \;+\; H_2 \;\;\rightarrow\;\; H_2^* \;\;\rightarrow\;\; H_2 \;+\; h\nu \qquad (11.12)$$

The cosmic ray induced spectrum is reproduced in Figure 11.10. It consists of a large number of discrete peaks, mostly due to H_2 Lyman and Werner band photons, with a weak underlying continuum. In order to estimate dissociation rates, coincidences between the cosmic-ray induced photons and the photodestruction cross sections have to be found.
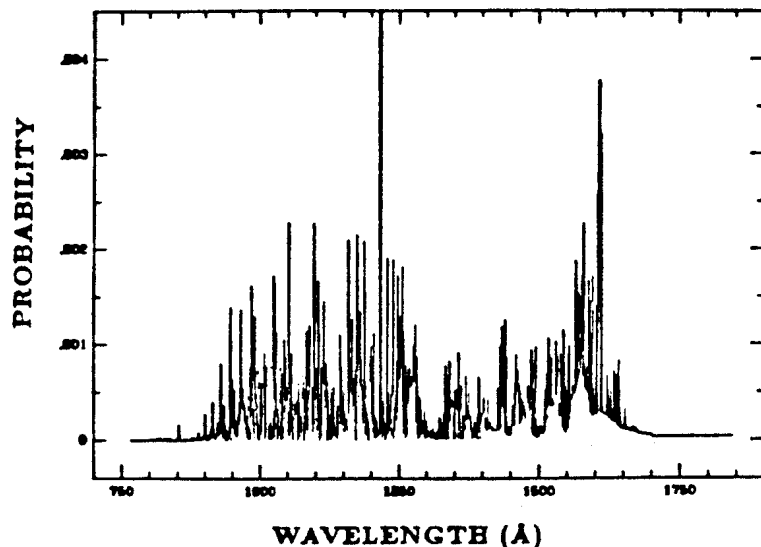
Figure 11.10– The emission spectrum of H_2 following excitation by cosmic-ray induced secondary electrons.

(iv) The Solar Radiation Field

The radiation that destroys molecules in the atmospheres of the planets, including the Earth, and in cometary atmospheres is provided by the Sun. The intensity is thus strongest in the visible, and drops very rapidly in the UV (Figure 11.11). For example, the average solar intensity at 5000 Å is a factor of about 10^5 larger than that at 1500 Å. Therefore **any** channel which lies very low in energy may dominate the photodissociation of the molecule in these atmospheres, even if it has a comparatively small cross section. The same channel may be completely negligible in the interstellar medium.

For example, the photodissociation of cometary OH is dominated by predissociation through the $A^2\Sigma^+$ channel, whereas the photodissociation of interstellar OH occurs mostly through higher channels, such as the $1^2\Sigma^-$ channel. In addition, there are a few resonance lines at shorter wavelengths, such as the Lyman-α line at 1215.6 Å, which may be effective in the solar spectrum. Note that the solar flux in the ultraviolet may vary by a factor of two or more between solar minimum and maximum. Also, in cometary atmospheres, the rate may depend on the heliocentric radial velocity of the comet, if the photodissociation occurs by discrete absorptions in a wavelength region where the solar intensity is varying rapidly with wavelength. This is called the *Swings effect.*

(e) Photodissociation of Isotopic Species

For the direct photodissociation mechanism, the cross sections for isotopic species are very similar to those for the main isotopes. For processes proceeding through line absorption, however, substantial differences may occur if the onset of predissociation of the isotopic species starts at a different energy level with, e.g., a lower oscillator strength than that of the principal species. For example, predissociation of the $A^2\Sigma^+$ state of OD starts at $\nu' = 3$ compared with $\nu' = 2$ for OH, so that the photodissociation of cometary OD is a factor of three slower than that of OH.
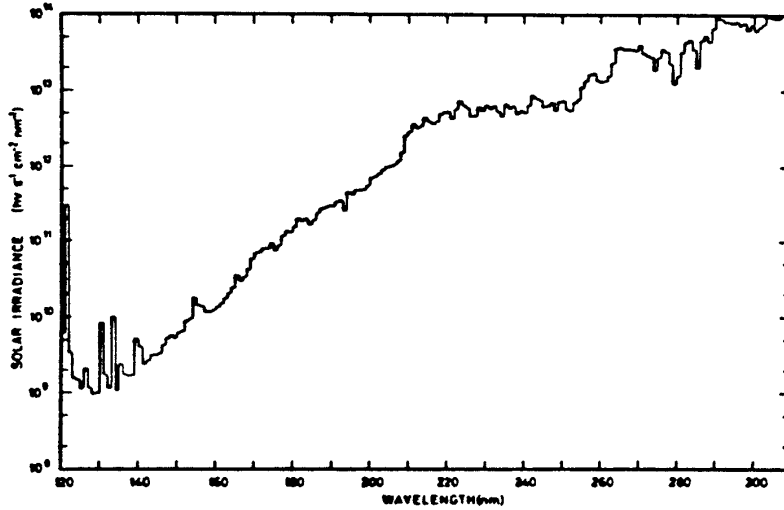
Figure 11.11– Spectral solar irradiance in the UV between 120 and 310 nm.

Additional differences can occur if the absorption lines become saturated. This is illustrated by the case of ^{12}CO, ^{13}CO, $C^{18}O$, ... in interstellar clouds. Because ^{12}CO is much more abundant than ^{13}CO, its lines become optically thick very rapidly, so that inside an interstellar cloud, ^{12}CO is much less rapidly photodissociated than ^{13}CO, $C^{18}O$, ... as Figure 11.12 shows. The calculation is complicated, however, by the fact that ^{13}CO lines in the (0,0) bands can still be effectively shielded by ^{12}CO inside the cloud, but not lines in with $\nu \geq 1$, owing to the larger isotope shift when non-zero vibrational quantum numbers are involved.
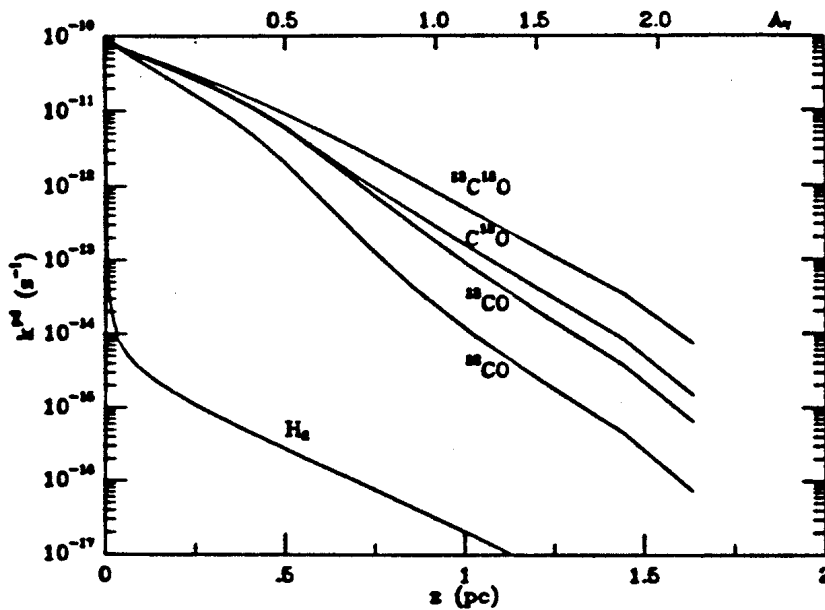

Figure 11.12– Photodissociation rates of CO and its principal isotopes as a function of depth into a cloud with a visual extinction of 5^m.
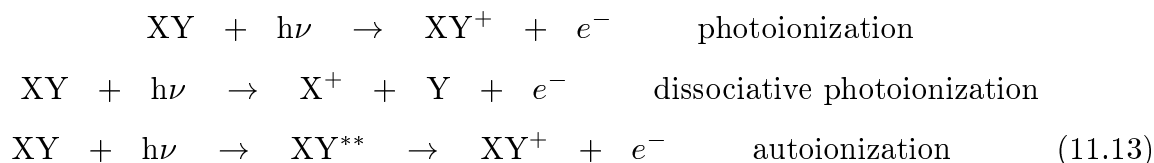
(f) Additional Considerations

All of the above photodissociation processes are more than just mechanisms to destroy a molecule. We have already seen that they can be a significant source of opacity, both line and continuum, thereby modifying the radiation field and hence the physical characteristics of an astrophysical environment. Closer to home, it is the photodissociation of ozone (O_3) in the stratosphere that is responsible for shielding the near-surface regions of the Earth from ultraviolet radiation. O_3 absorbs strongly in the Hartley $^1B_2 - {}^1A_1$ transition from 2000 – 3000 Å, and weakly in the visible through the Huggins and Chappius bands. Figure 11.13 illustrates the relevant section through the O_3 potential surfaces, together with the measured absorption spectra. Figure 11.14 summarizes the most important sources of opacity in the Earth's atmosphere.

In the atmospheres of the outer planets and that of Titan, CH_4 is so abundant that it prevents radiation at $\lambda <$1600 Å from deeper penetration due to its strong continuous absorption (see Figure 11.8). Atoms resulting from photodissociation events can have significant kinetic energy, which can **heat** the ambient gas just as photoelectrons do. The photodissociation of O_2 through the Schumann-Runge continuum is the principal heating source of the thermosphere. Note that photodissociation can also leave the product species in an excited electronic state, which can subsequently decay through characteristic emission-line radiation.

(g) Photoionization

Absorption of a photon with an energy above the lowest ionization threshold can result in both photoionization and photodissociation of the molecule. The ionization processes that can occur for a diatomic molecule XY are

$$XY \; + \; h\nu \; \rightarrow \; XY^+ \; + \; e^- \qquad \text{photoionization}$$

$$XY \; + \; h\nu \; \rightarrow \; X^+ \; + \; Y \; + \; e^- \qquad \text{dissociative photoionization}$$

$$XY \; + \; h\nu \; \rightarrow \; XY^{**} \; \rightarrow \; XY^+ \; + \; e^- \qquad \text{autoionization} \qquad (11.13)$$

As for atoms, the photoionization cross section is finite at threshold and generally consists of a smooth background with superposed resonances due to interactions with Rydberg states of the neutral molecule. The percentage of absorptions leading to dissociative photoionization is usually low at threshold, $<$5-10%, but increases with photon energy.

Reviews on Photodissociation Processes:

van Dishoeck, E.F. 1987, in *Astrochemistry*, IAU Symposium 120.

Kirby, K and van Dishoeck, E.F. 1988, *Adv. Atom. Mol. Phys.* **25**, 437.

van Dishoeck, E.F. 1988, in *Rate Coefficients in Astrochemistry*, (eds. T.J. Millar & D.A. Williams).
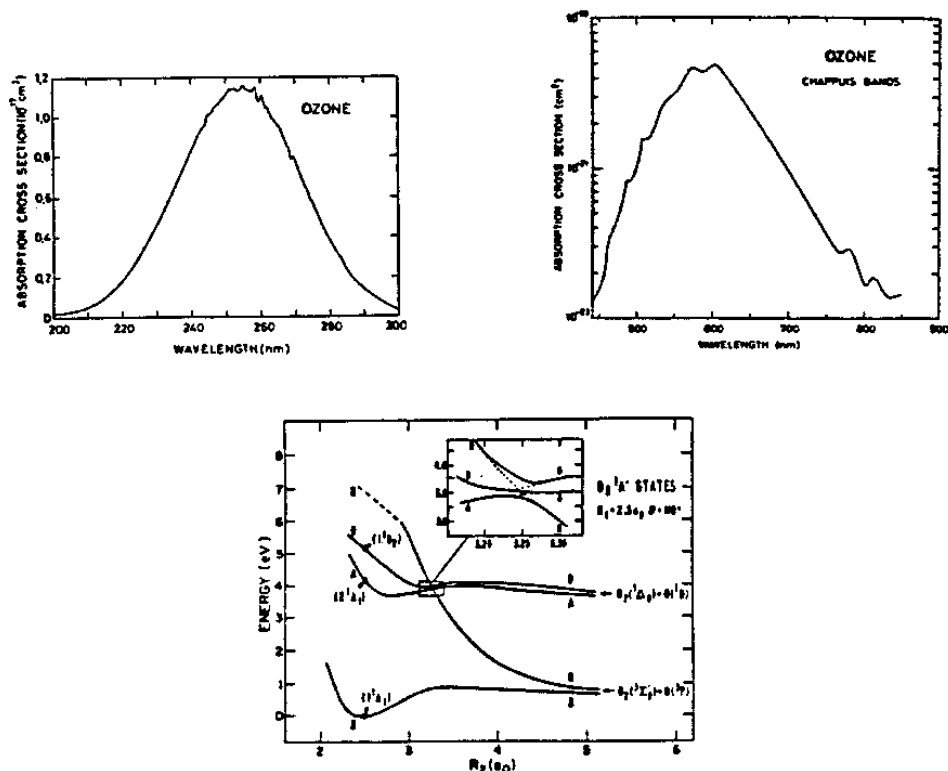
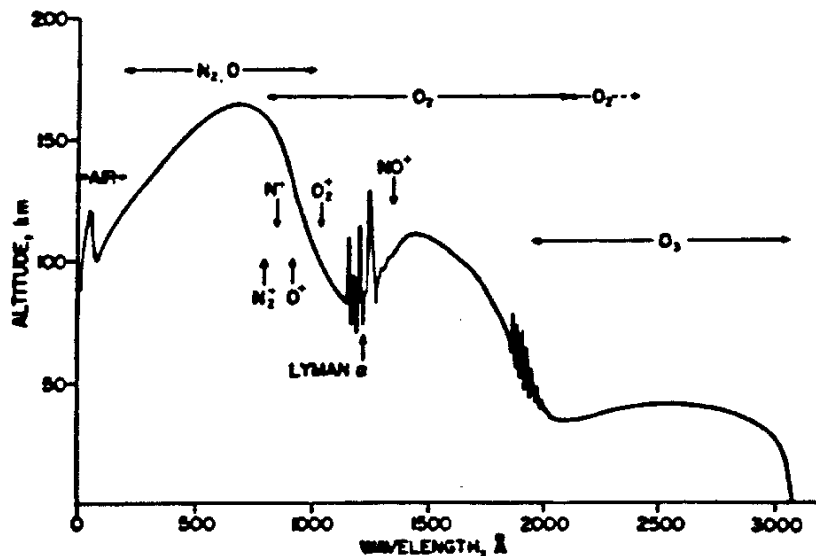**Figure 11.13**– Absorption cross sections and potential curves for O_3.

Figure 11.14– Depth of penetration of solar radiation in the ultraviolet as a function of λ. The line shows the altitude of unit optical depth, vertical arrows denote ionization limits.
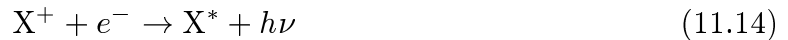
XI. MOLECULAR PROCESSES (completed)

2. Dissociative Recombination

Although the destruction of neutral molecules is dominated by photodissociation, molecular ions are usually more rapidly destroyed by recombination with electrons.

a) Mechanism

For an atomic ion, recombination with electrons is accompanied by the emission of a photon

$$X^+ + e^- \to X^* + h\nu \tag{11.14}$$

where usually the neutral atom is formed in an excited state. As we have seen in § IV.B, this radiative recombination process is relatively slow, with a typical rate coefficient of the order of $10^{-12} \mathrm{cm}^3 \mathrm{s}^{-1}$ at T=100 K, decreasing as $T^{-1/2}$ with increasing temperature.

In molecular ions, the efficiency of radiative recombination may be enhanced by resonances due to the rotational and vibrational levels of excited electronic states lying above the ionization threshold. An example is illustrated in Figure 11.15b, where an electron with energy E approaching a molecular ion XY^+ in its ground state can be captured in an excited vibrational level of a high-lying state of the neutral molecule XY^*, which can subsequently radiate to a lower state of the neutral molecule. This is the molecular analogue of di-electronic recombination in atoms.

For molecular ions, however, "dissociative recombination"

$$XY^+ + e^- \to X + Y \tag{11.15}$$

is usually much more rapid than radiative recombination.

In the "direct" process, illustrated in Figure 11.15a, an electron with energy E directly excites a transition from the stable ion into a repulsive excited state of the neutral molecule which crosses the potential curve of the ion. The excited state subsequently dissociates into the atoms X+Y.

An "indirect" mechanism is depicted in Figure 11.15b, in which the electron is temporarily captured in the excited neutral electronic state XY^* potential curve, and subsequent separation of the nuclei occurs.

b) Rate coefficients

Measurements of dissociative recombination processes have been performed for a number of astrophysically important ions. A useful review containing a list of rate coefficients has been presented by Mitchell and McGowan 1983, in 'Physics of Ion-Ion and Electron-Ion Collisions' (eds. F. Brouillard and J. W. McGowan) p. 279. They are typically 10^{-6} $(T/100)^{-1/2}$ $\mathrm{cm}^3 \mathrm{s}^{-1}$. Most experiments have been performed at room temperature and presumably pertain to ions distributed over various vibration-rotation states. The majority of these ions are expected also to recombine rapidly at interstellar temperatures, where only the lowest energy levels are populated. Some exceptions, however, have recently been found. In particular, the dissociative recombination of the H_2^+, HeH^+ and possibly CH^+ ions may be slow at low temperatures because no repulsive potentials crossing that of the ground-state ion have been identified.
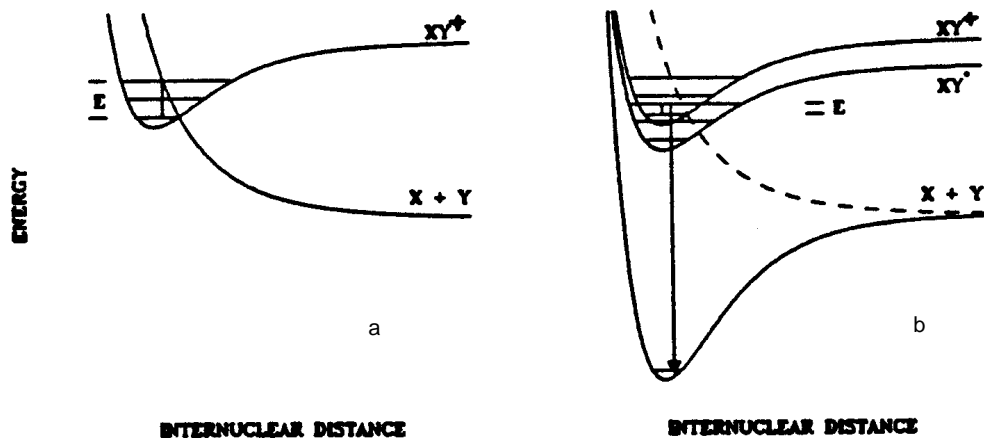
Figure 11.15– Potential energy curves illustrating the processes of a: direct dissociative recombination; and b: indirect dissociative recombination and radiative recombination.

c) Dissociative recombination of H_3^+

H_3^+ is the critical molecular ion in dense interstellar clouds and in the ionospheres of the Jovian planets, thanks to the overwhelming abundance of molecular hydrogen in these regions. Accordingly, the dissociative recombination rate of H_3^+ at low temperatures

$$H_3^+ + e^- \quad \rightarrow \quad H_2 + H \text{ or } H + H + H \tag{11.16}$$
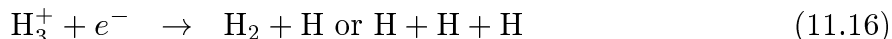
is currently the subject of considerable discussion since it helps to determine the ionization balance in such regions. Some experiments claim that it is extremely slow at low temperatures, $k_{dr} < 10^{-10}$ cm^{3}s^{-1}, whereas other experiments suggest $k_{dr} \lesssim 10^{-7}$ cm^{3}s^{-1}. Whether or not the dissociative recombination of H_3^+ is rapid is important not only in the chemistry of diffuse interstellar clouds, but also in Jovian ionospheric chemistry.

H_3^+ can be formed very rapidly in gas composed primarily of hydrogen through the reaction

$$H_2^+ + H_2 \rightarrow H_3^+ + H \tag{11.17}$$

where in interstellar clouds, the H_2^+ ions result from cosmic ray ionization of H_2, and in ionospheres from photoionization and electron-impact ionization of H_2. Most models of the ionosphere of Jupiter have assumed that the process (11.16) proceeds rapidly, so that in equilibrium, H^+ is the major ion rather than H_3^+. However, if (11.16) proceeds slowly, H_3^+ may be the major consituent of the ionosphere! The recombination coeffient depends on the vibrational distribution of the ionospheric H_3^+ ions, so that vibrational excitation and de-excitation processes are a significant part of the chemistry of the Jovian ionosphere.

H_3^+ was first detected in the auroral regions of the Jovian ionosphere through high resolution iIR observations of the $2\nu_2$ band at 2 μm (see Figure 11.16; Drossart *et al*. 1989, *Nature* **340**, 539). The inferred rotational population distribution can be characterized by a $T_{ROT}(H_3^+)$ in the range 1000-1200 K. The same spectrum also shows the H_2 Δv=1 ro-vibrational bands (see also Figure 9.3). The H_2 excitation is characterized by a temperature $T \approx 750\pm300$ K. Note that the H_3^+ lines are only detected in the auroral spectrum, but
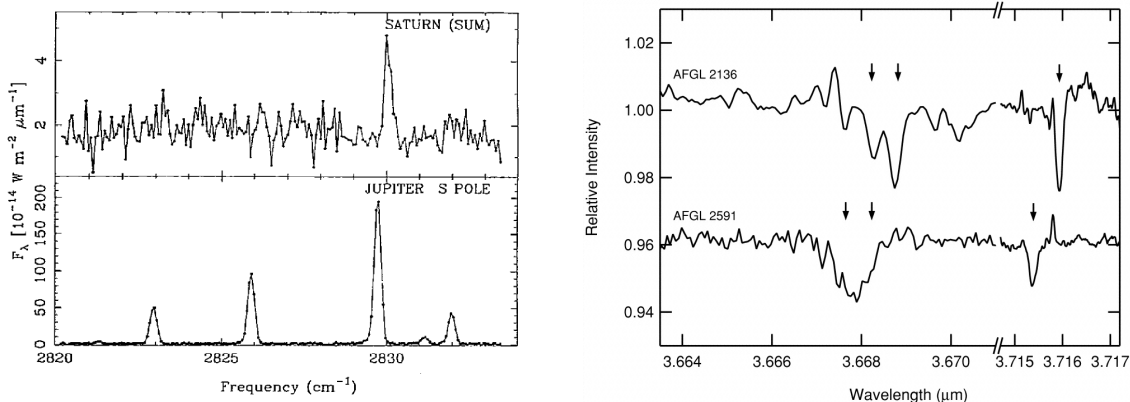
Figure 11.16– (Left) Infrared emission spectra of H_3^+ from the polar aurorae of Saturn and Jupiter; (Right) Absorption spectra of H_3^+ toward the massive young stellar objects AFGL 2136 and 2195.

not in non-auroral spots. This may result from the fact that the electrons resulting from the auroral precipitation can maintain a large abundance of H_3^+ through reaction (11.17), even if the dissociative recombination of H_3^+ is fast.

Thanks to continuing improvements in IR detector arrays and to the construction of large aperture IR-optimized telescopes, it has recently become possible to detect H_3^+ in both diffuse clouds and dense interestellar clouds (Figure 11.16, right). The concentration of H_3^+ is found to be largely invariant to environment and density, and forms a challenge to the existing chemical theories. Part of the explanation may lie in a transition of the dominant destruction reaction from dissociative recombination (eq. 11.16) to proton transfer to abundant neutral species such as CO or N_2 in dense clouds (more in a bit).

d) Product branching ratios

A major uncertainty in models of interstellar clouds and planetary atmospheres is the nature of the neutral products of the dissociative recombination of polyatomic ions. In the absence of any laboratory data or good theory, most models have assumed that either a single hydrogen atom is detached, or that H and H_2 are formed in equal amounts in the dissociative recombination:

$$XH_n^+ + e^- \rightarrow XH_{n-1} + H$$

$$\rightarrow XH_{n-2} + H_2. \tag{11.18}$$

For example, most models assume that both H_2O and OH are formed by:

$$H_3O^+ + e^- \rightarrow H_2O + H$$

$$\rightarrow OH + H_2. \tag{11.19}$$
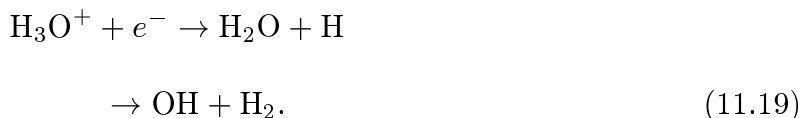
Some theoretical calculations have suggested that H_2O is formed exclusively in this reaction. However, Herd, Adams and Smith 1990, *Ap. J.* **349**, 388 have succeeded in measuring the branching ratio of H_3O^+ dissociative recombination for the first time. They find that the majority of the recombinations, about 65%, leads to OH.

– 273 –

References:
Adams and Smith 1987, in 'Astrochemistry', IAU Symposium 120
Adams and Smith 1988, in 'Rate coefficients in Astrochemistry'
Bates and Herbst 1988, in 'Rate coefficients in Astrochemistry'

e) Astrophysical considerations

The realization that dissociative recombination may be an important destructive mechanism of molecular ions was realized already by Bates and Massey in 1947 in early ionospheric analyses. They recognized that radiative recombination

$$O^+ + e^- \rightarrow O + h\nu \tag{11.20}$$

is a very slow process, and that charge-transfer of O^+ to O_2 to form a molecular ion O_2^+, followed by dissociative recombination

$$O_2^+ + e^- \rightarrow O + O \tag{11.21}$$

proceeds much more rapidly. However, at the time that Bates and Massey introduced the process, there was no quantitative evidence on its efficiency. It was not until 1970 that the first reliable measurements of the dissociative recombination of the atmospheric ions NO^+, N_2^+ and O_2^+ were made.
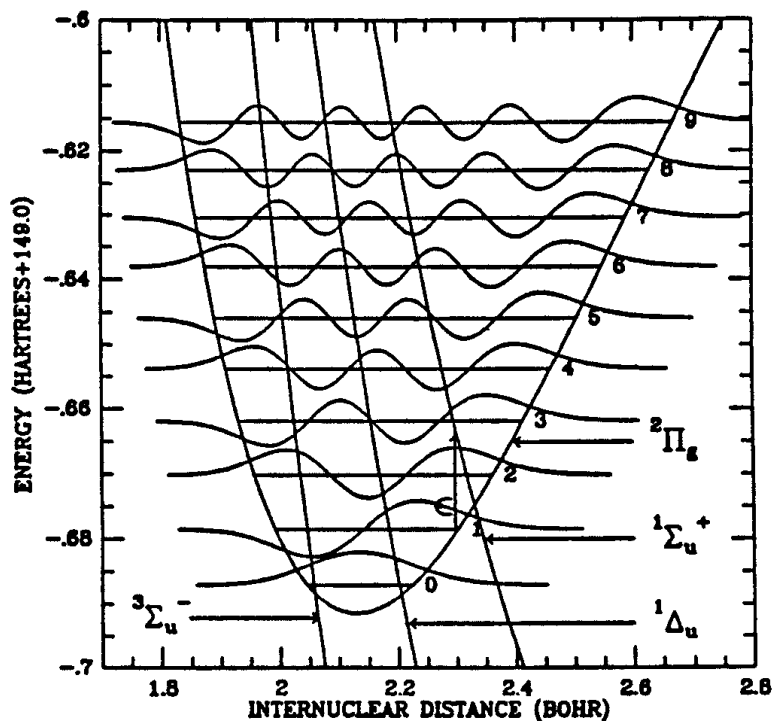

Figure 11.17– The three most important potential energy curves for dissociative recombination leading to $O(^1D)$. The vibrational wavefunctions are each plotted on the same scale and are obtained from the numerical solution of the 1D Schrödinger equation.

The study of these processes is even more challenging theoretically, since it involves the calculation of highly-excited states of the neutral product molecule (see Figure 11.17).
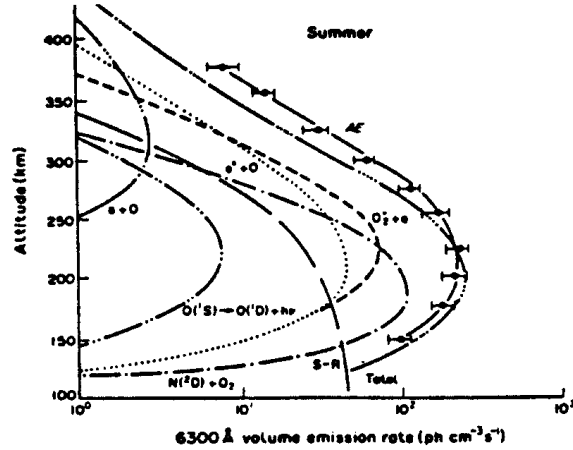
Figure 11.18– Daytime O I 6300Å volume emission rates as a function of altitude (7/74).

Nevertheless, the calculations have progressed to the point that they can provide reliable estimates of the amount of O atoms produced in the excited ^{1}S and ^{1}D states. For more details, see Guberman 1989, in 'Dissociative Recombination: Theory, Experiment and Applications' ed. J. B. A. Mitchell and S. L. Guberman.

Because the dissociative recombination can lead to excited state atoms, they can be an important source for atomic line emission. Indeed, most of the O(^{1}D) red line and O(^{1}S) green line emission in the ionospheric E and F regions result from the dissociative recombination of O_2^+. Figure 11.18 demonstrates that at high altitudes, most of the day time O I red line emission comes from this process, whereas at lower altitudes, electron-impact excitation of O by photoelectrons, and photodissociation of O_2 in the Schumann-Runge (S-R) system is important. Similarly, most of the N(^{2}D) emission at 5200Å in the upper atmosphere results from the dissociative recombination of NO^+.

As in the process of photodissociation, the product atoms are produced with a significant amount of kinetic energy, which can *heat* the gas. This is a significant heating source, not only of the Earth's ionosphere, but also of that of other planets. An example is shown in Figure 11.19 for the atmosphere of Venus. The figure shows the principal heating sources of the Venusian thermosphere as a function of altitude. At low altitudes (<130 km), photodissociation of CO_2 is the principal heating source, but at higher altitudes (>135 km), dissociative recombination of O_2^+ dominates.
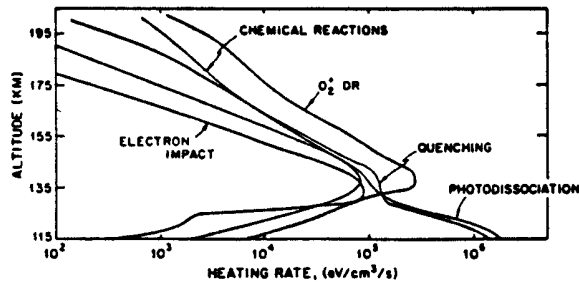

Figure 11.19– Altitude profiles of heating rates due to the major sources of neutral heating in the Venusian thermosphere from 115 to 200 km.

– 275 –

Because the product atoms may possess considerable kinetic energy, they may *escape* from the planet's atmosphere. Inspection of the various elemental abundances on the planets show that some elements have been lost from the atmospheres over time. The best known examples are the loss of H and He from the atmospheres of the Earth, Venus, and Mars, but detailed analyses of, for example, the initial nitrogen reservoir on Mars show that nitrogen must have escaped from the planet as well. The dominant source in this case is probably the dissociative recombination of N_2^+. Because the kinetic energies for the isotopic species ^{15}N and ^{14}N are different, the escape rates for these two species differ substantially leading to anomalous $^{15}N/^{14}N$ ratios of the nitrogen that is left on Mars. Table 11.1 summarizes the possible non-thermal processes that can lead to escape.

Table 11.1– Nonthermal Processes Leading to Escape[a]

Process	Examples	Product	Remarks
1. Charge exchange	(a) $H + H^{+*} \rightarrow H^+ + H^*$	N	
	(b) $O + H^{+*} \rightarrow O^+ + H^*$		
2. Dissociative recombination	(a) $O_2^+ + e \rightarrow O^* + O^*$	N	Energy divided equally
	(b) $OH^+ + e \rightarrow O + H^*$		H takes nearly all the energy
3. Impact dissociation	(a) $N_2 + e^* \rightarrow N^* + N^*$	N	e* may be a photoelectron or an accelerated one
Photodissociation	(b) $O_2 + h\nu \rightarrow O^* + O^*$		
4. Ion-Neutral reaction	$O^+ + H_2 \rightarrow OH^+ + H^*$	N	
5. Sputtering or	$Na + S^{+*} \rightarrow Na^* + S^{+*}$	N	Sputtering requires kilovolt or greater energies
knock-on	$O^* + H \rightarrow O^* + H^*$		Knock-on requires much less (lighter, much)
6. Solar-wind pickup	$\begin{cases} O + h\nu \rightarrow O^+ + e \\ O^+ \text{ picked up} \end{cases}$	I	Also electron impact
			Also magnetospheric wind for satellites
7. Ion escape	H^{+*} escapes	I	Requires open magnetic-field lines
8. Electric fields	$X^+ + eV \rightarrow X^{+*}$	I	Generates fast ions and electrons that participate in other processes

[a] An asterisk represents excess kinetic energy. In the third column, N means neutral and I means ion.

3. Chemical Reactions

Chemical reactions both destroy and form molecules at the same time. Two types of reactions can be distinguished:

$$X + YZ \rightarrow XY + Z \quad \text{neutral} - \text{neutral}$$

$$X^+ + YZ \rightarrow XY^+ + Z \quad \text{ion} - \text{molecule} \tag{11.22}$$

a) Neutral-neutral reactions

The rate coefficients for neutral-neutral reactions are usually small at low temperatures and vary considerably from species to species. This is because the long-range attraction between the reactants is only the relatively weak van der Waals interaction, which decreases as R^{-6} at large R. In addition, potential barriers may occur in either the entrance or exit channel (that is, closer to the reactants or products, c.f. Figure 11.20). This results in an exponential decrease of the rate coefficient at low temperatures, even if the reaction is exothermic (or exoergic meaning net energy output) and proceeds rapidly at room temperature. Thus, neutral-neutral reactions are not invariably important in cold interstellar clouds. Exceptions are reactions such as
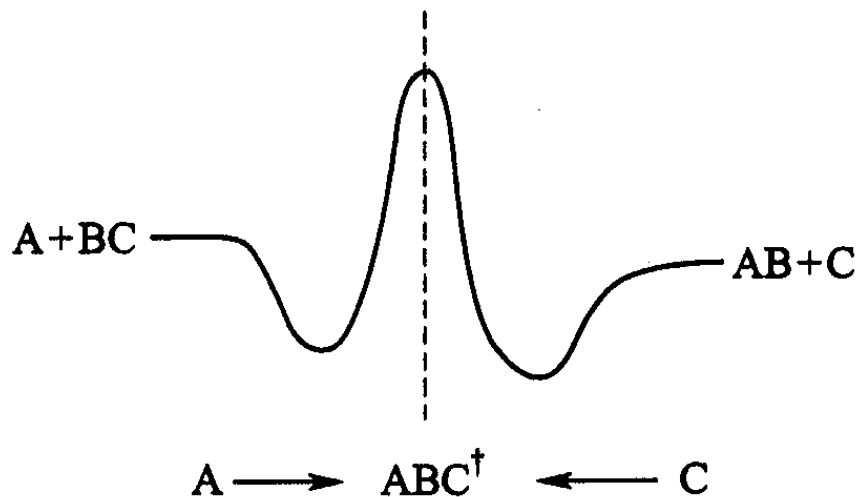
$$O + OH \rightarrow O_2 + H \tag{11.23}$$

Figure 11.20– Schematic illustration of the potential energy along a possible reaction path for two neutral species. For fast ion-molecule reactions the activation barrier is overcome by the collisional energy.

$$N + C_2 \rightarrow CN + C \tag{11.24}$$

$$C + O_2 \rightarrow CO + O \tag{11.25}$$

which may contribute to the formation of O_2 and CN in interstellar clouds, as well as the removal of atomic C. Reaction (11.23) is of particular interest. A detailed theoretical study of it has recently been performed by Graff (1989, *Ap. J.* **339**, 239), and suggests that the reaction is rapid at low temperatures. Only a few neutral-neutral rates have been measured at low temperatures in the laboratory. They increase approximately as $T^{0.17}$ with increasing temperature.

b) Ion-molecule reactions

In contrast, exothermic reactions between ions and neutrals proceed very rapidly at low temperatures, owing to the strong long-range attraction between the ion and the (induced) dipole of the molecule. Simple estimates of the rate can be made based on the long-range polarization potential:

$$V(R) = -e^2\alpha/2R^4 \tag{11.26}$$

where α is the polarizability of the neutral molecule. In the classical capture theory, the effective potential is

$$V_{eff}(R) = -\frac{e^2\alpha}{2R^4} + \frac{\mu b^2 v^2}{2R^2} \tag{11.27}$$

where μ is the reduced mass of the system. This effective potential has a maximum of $(\mu b^2 v^2)^2/8\alpha e^2$. This barrier can only be surmounted if the kinetic energy of the collision is larger:

$$\frac{1}{2}\mu v^2 > (\mu b^2 v^2)^2/8\alpha e^2. \tag{11.28}$$

This leads to the critical impact parameter

$$b_c = (4\alpha e^2/\mu v^2)^{1/4}. \tag{11.29}$$

If $b < b_c$, the ion can get close to the molecule so that a reaction may take place, whereas for $b > b_c$, the two systems stay far away on average. Figure 11.21 illustrates these two situations. If it is assumed that every close collision leads to a reaction, then the cross section for reaction is

$$\sigma = \pi b_c^2 \tag{11.30}$$

and the collisional rate coefficient is

$$k_L = \sigma v = 2\pi(\alpha e^2/\mu)^{1/2}. \tag{11.31}$$

Note that the so-called 'Langevin' rate coefficient is *independent of temperature*. For most reactions, it is of order $10^{-9}\mathrm{cm^3 s^{-1}}$.
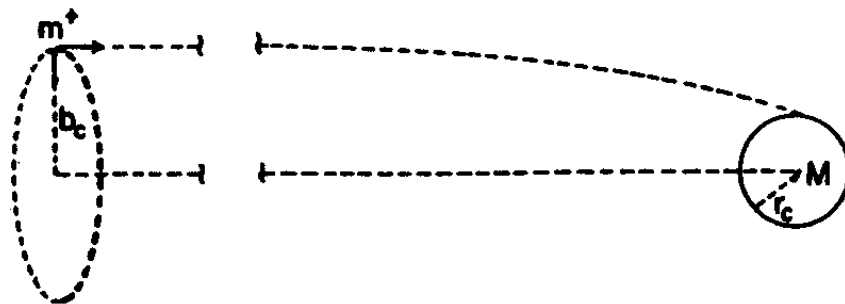

Figure 11.21– Schematic illustration of an ion-molecule collision.

Many ion-molecule reactions have been studied in the laboratory, and for exothermic reactions, the measured rate coefficients agree well with those predicted by the simple Langevin theory. An extensive compilation of rate coefficients has been given by Anicich and Huntress (1986, *Ap. J. Suppl.* **62**, 553). Still, only few reactions have been measured at interstellar temperatures. It is usally assumed that if a reaction proceeds rapidly at room temperature, it will do so at low temperatures as well, whereas if the reaction is significantly slower than the Langevin rate at room temperature, it is probably slightly endothermic (net input) and thus negligible at interstellar temperatures. Some exceptions to this simple rule are known, however. The most famous example is the reaction

$$\mathrm{NH_3^+ + H_2 \rightarrow NH_4^+ + H} \tag{11.32}$$

which may be an important link in the formation of ammonia in interstellar clouds, and in the atmosphere of Titan. The measured rate coefficient for this reaction is illustrated in Figure 11.22a as a function of temperature. The reaction is exoergic, but its rate coefficient is relatively small at room temperature and decreases rapidly with lower temperatures down to 100K. This behavior is indicative of a barrier along the reaction path, and led to the suggestion that the reaction would be negligibly slow in cold interstellar clouds with
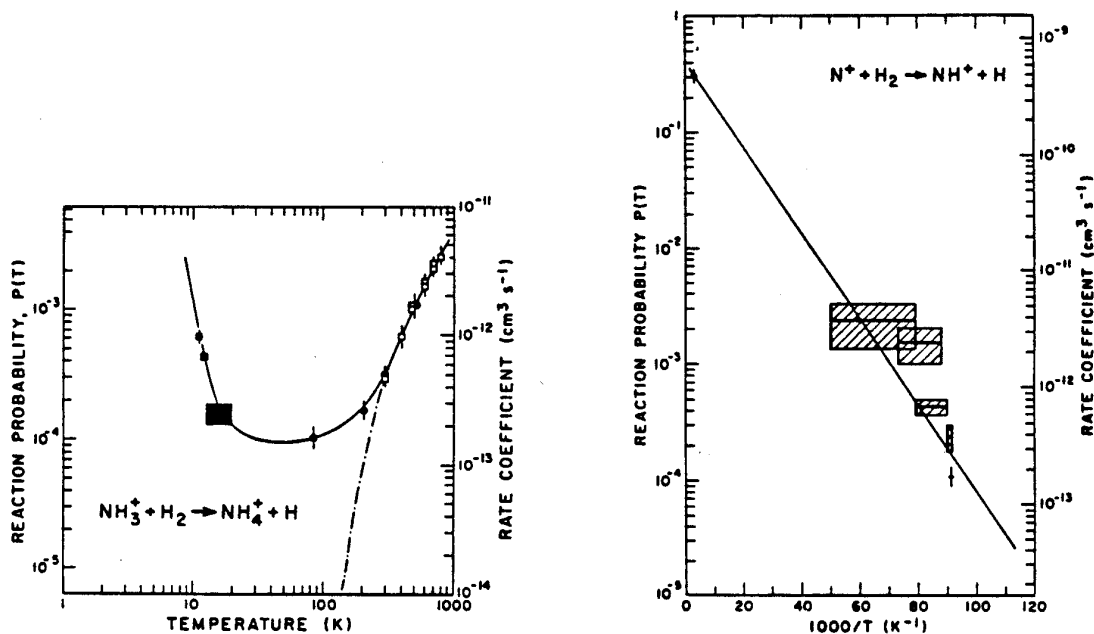
Figure 11.22– (Left, a) Measured rate coefficent for the reaction $NH_3^+ + H_2 \rightarrow NH_4^+ + H$ as function of temperature. The dot-dashed curve was used previously in models of interstellar clouds. (Right, b) Measured rate coefficient for the reaction $N^+ + H_2 \rightarrow NH^+ + H$ as a function of temperature.

$T \approx$ 10-20 K. Quite unexpectedly, subsequent experiments showed that the rate coefficient increases significantly at low temperatures $T <$ 100 K. This unusual temperature behavior can be explained by the formation of a long-lived, pre-barrier, complex at low temperatures, during the lifetime of which tunneling through the barrier is enhanced.

Another instructive example is provided by the reaction

$$N^+ + H_2 \rightarrow NH^+ + H \tag{11.33}$$

which is an initiating step in the formation of nitrogen-bearing molecules in interstellar clouds. The measured rate coefficient is shown in Figure 11.22b (right) as a function of temperature. Although this reaction proceeds rapidly at room temperature, it continues to decrease at low temperatures. Recent experiments have demonstrated that the reaction is actually endoergic by a small amount of the order of 10meV, leading to a measured rate coefficent of only $10^{-14} cm^3 s^{-1}$ at 10 K. It should be noted, however, that again the experimental results pertain to normal hydrogen (with three times as much *ortho*-H_2 as *para*-H_2) whereas the cloud models require rate coefficients for reaction with *para*-H_2 only. It is not clear whether the rate coefficients will be significantly smaller in the latter case.

The simple Langevin theory with temperature-independent rate coefficients of 10^{-9} $cm^3 s^{-1}$ is strictly appropriate only for reactions between ions and non-polar molecules. It was realized already more than a decade ago that the long-range interaction between an ion and a molecule with *permanent* dipole moment is stronger than in the former case, so that the rate coefficients are expected to increase at low temperatures. This behavior has

– 279 –

recently been confirmed for important interstellar reactions such as:

$$C^+ + H_2O \rightarrow HCO^+ + H \qquad (11.34)$$

$$H_3^+ + HCN \rightarrow H_2CN^+ + H_2. \qquad (11.35)$$

These experiments together with further theoretical work, indicate that the ion-polar molecule rate coefficients may increase at low $T \approx$ 10-20 K by 1-2 orders of magnitude over the Langevin values.

The rate coefficients for both neutral-neutral and ion-molecule reactions may also be affected by the rotational population distribution of the reactants of the fine-structure excitation of the atoms. Laboratory measurements usually refer to thermal distributions over the various energy levels, whereas in cold interstellar clouds, most molecules reside only in the lowest few levels. Thus, care must be taken in the use of the experimental values.

Isotope fractionation processes

Because the isotopic species have slightly different zero-point vibrational energies (see Eqn 7.40), some ion-molecule reactions may proceed preferentially in the direction of the heavier molecule. A well-known example in interstellar chemistry is the isotope exchange reaction

$$^{13}C^+ + ^{12}CO \rightleftharpoons ^{13}CO + ^{12}C^+$$
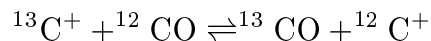
which is exothermic in the forward direction by about 36 K, owing to the difference in zero-point vibrational energy between ^{12}CO and ^{13}CO. Thus, at low temperatures $T <$30K, the ^{13}CO abundance in enhanced compared with the overall $[^{13}C]/[^{12}C]$ ratio of carbon in all forms; ^{13}CO is said to "fractionated." At higher temperatures $T \geq$50K, the reverse reaction occurs nearly as fast as the forward reaction so that no fractionation occurs.

Another extremely important example is the reaction

$$H_3^+ + HD \rightleftharpoons H_2D^+ + H_2$$
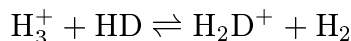
which is exothermic by ~150 K, and which leads eventually to considerable deuterium fractionation in organic molecules in interstellar clouds. Indeed, at the temperatures prevailing in the cores of dense molecular clouds ($T_{kin} \approx 10 - 20$ K), the enhancement can be nearly four orders of magnitude, as is illustrated by the D/H values measured in a variety of tracers in both interstellar clouds and solar system objects and summarized in Figure 11.23. Proton transfer to neutrals like CO leads directly to deuterium enhancement in the DCO^+/HCO^+ ratio, while in species like water both the proton transfer and dissociative recombination steps must be modeled to understand the HDO/H_2O ratio.

References: Clary, D. C. 1988; Rowe B. R. 1988; Smith and Adams 1988 in 'Rate Coefficients in Astrochemistry.'
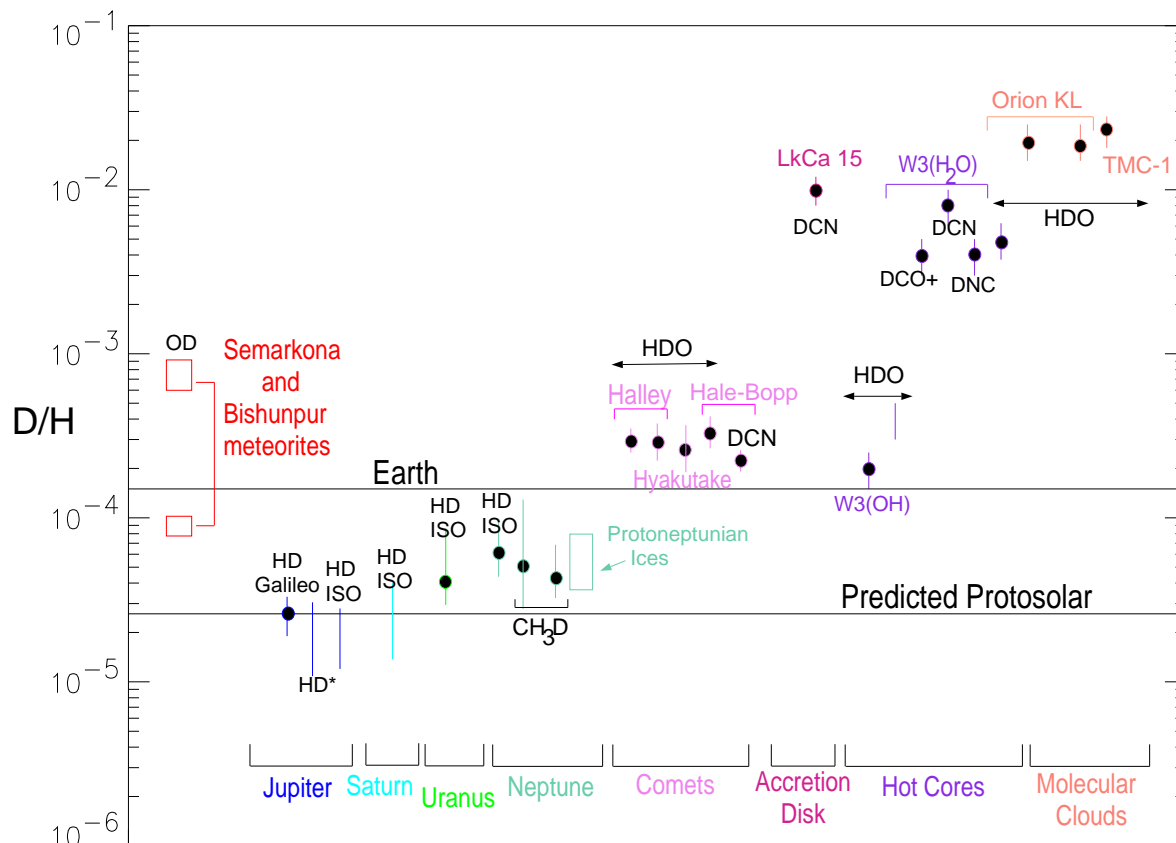
Figure 11.23– Values of D/H measured in a range of interstellar and solar system environments. For the interstellar cases, the highests values of D/H are observed in ions such as DCO^+/HCO^+ or in small organic molecules such as HCN/DCN.

c) Charge-transfer reactions

Atomic charge transfer processes,

$$X + Y^+ \rightarrow X^+ + Y \tag{11.36}$$

have already been discussed in § V.6. At low temperatures, the process can be best described in terms of the potential curves of the molecule XY^+ that characterizes the interaction between the two atomic species (see Figure 11.24). The potential curves correlating with the reactants and products $X+Y^+$ and X^++Y are usually of the same symmetry, and can therefore not cross in the Born-Oppenheimer approximation. However, at the location of the avoided crossing, the character of each of the states is changing rapidly, so that the Born-Oppenheimer approximation breaks down. It is precisely the coupling between the nuclear and electronic motions that allows the process to occur. A pseudo-molecule X^+-Y therefore has a large probability for 'hopping' (during a collision) over to the pseudo-molecule X-Y^+ at the avoided crossing.

Whether or not a charge-transfer process is fast thus depends on the availability of suitable potential energy curves which have avoided crossings. The same holds if one of the reactants is a molecular species. For most complex systems, charge transfer is usually
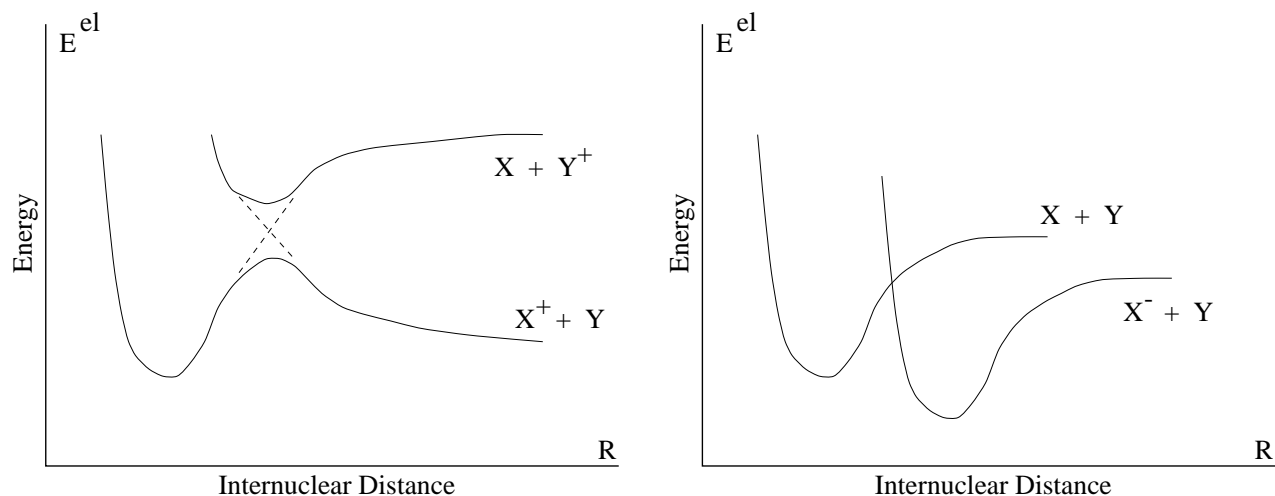
Figure 11.24– (Left) Potential energy curves explaining the process of charge-transfer in diatomic molecules. **Figure 11.25**– (Right) Potential energy curves illustrating the process of associative detachment.

rapid, $k \approx 10^{-9}$ cm^{3}s^{-1}, but a notable exception is the case

$$\mathrm{He}^+ + \mathrm{H}_2 \rightarrow \mathrm{products} \qquad (11.37)$$

which despite its large exothermicity has a rate coefficient at 80 K of only 10^{-13} cm^{3}s^{-1}.

d) Negative ion reactions

As for dissociative recombination, the process of "associative detachment"

$$\mathrm{X}^- + \mathrm{Y} \quad \rightarrow \quad \mathrm{XY} + e^- \qquad (11.38)$$

occurs rapidly, if the negative ion and the neutral atom approach along a potential curve which intersects a potential curve of the neutral species (see Figure 11.25). Because the transition is radiationless, if occurs at a high rate. The process

$$\mathrm{H}^- + \mathrm{H} \quad \rightarrow \quad \mathrm{H}_2 + e^- \qquad (11.39)$$

is of particular astrophysical importance.

e) Mutual neutralization

$$\mathrm{X}^+ + \mathrm{Y}^- \quad \rightarrow \quad \mathrm{X} + \mathrm{Y} \qquad (11.40)$$

also proceeds rapidly, but is usually not important in interstellar clouds due to the low degree of ionization. However, it is important in ionospheric chemistry.
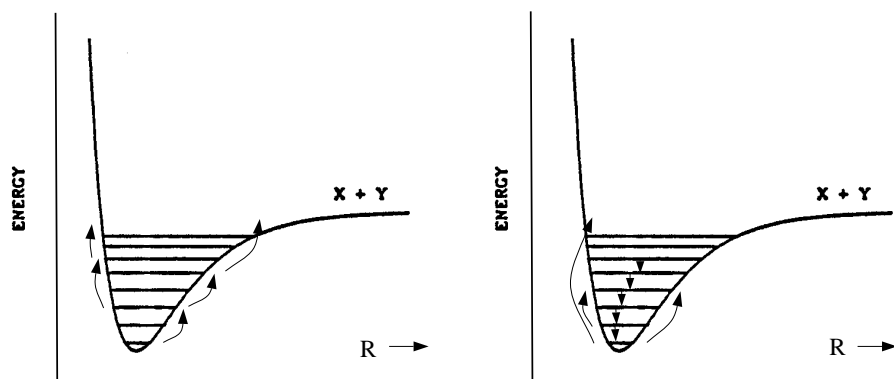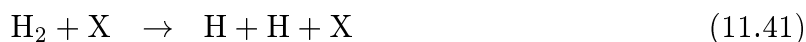
Figure 11.26– Potential energy curves explaining the process of collision-induced dissociation in the high-density regime (left, a) and the low-density regime (right, b).

4. Collision-Induced Dissociation

In warm molecular gas at temperatures of a few thousand degrees, molecules such as H_2 are destroyed by collision-induced dissociation:

$$H_2 + X \quad \rightarrow \quad H + H + X \tag{11.41}$$

where X=H, He or H_2. At high densities, the process occurs through collisional excitations into the vibrational continuum from the array of vibration-rotation levels populated by collisions (see Figure 11.26a). At lower densities, collisions are infrequent, and radiative stabilization occurs, in which the excited vibration-rotation levels can decay by spontaneous emission before collisional dissociation occurs. In this regime, the rate coefficient becomes a function of density, and in the limit, the rate is determined by direct collisional excitation from the lowest dipole moment, its radiative transitions are slow, so that the higher vibration-rotation levels remain populated. In contrast, in a molecule with a permanent dipole moment such as CO, the excited vibration-rotation levels decay rapidly, even at relatively high densities. Thus, H_2 is much more easily destroyed than CO by collisions.

Ref. Roberge and Dalgarno 1982, Ap. J. **255**, 489.

5. Radiative Association

a) Mechanisms

If the formation of a molecule out of two smaller species occurs entirely in the gas phase, it must be accompanied by the emission of a photon because of energy and momentum conservation. In this process of radiative association, the two smaller units come together to form an intermediate complex. This unstable complex can then either redissociate into the reactants, or be stabilized through the emission of a photon

$$X + Y \quad \rightleftharpoons \quad (XY)^* \quad \rightarrow \quad XY + h\nu. \tag{11.42}$$
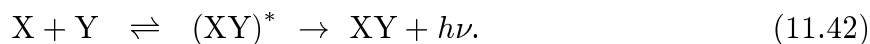
The processes for the formation of a diatomic molecule are illustrated in Figure 11.27. Note that radiative association can be considered to be the inverse process of photodissociation.
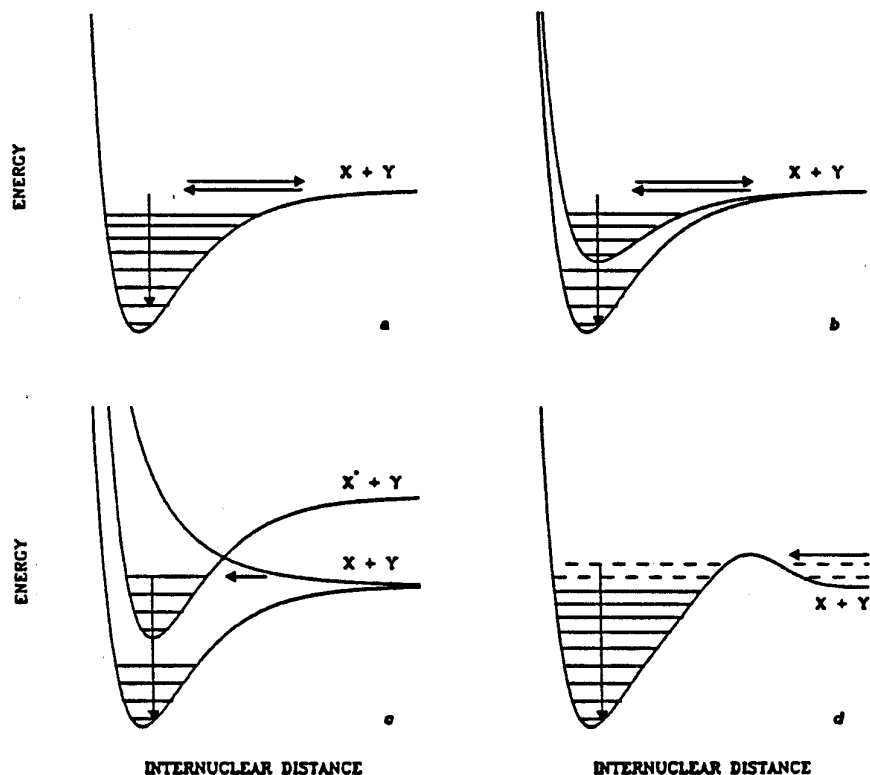
Figure 11.27– Potential energy curves illustrating the process of radiative association. a: Radiative association through the ground state vibrational levels; b: Radiative association involving an excited electronic state; c: Radaitive association through inverse predissociation; d: Radiative association through inverse vibrational predissociation.

In the simplest process of radiative association, the two atoms approach each other along the ground state potential energy curve of the molecule, and only photons within the vibrational levels of the ground electronic state can be emitted. It is easily demonstrated that this process is very inefficient: the typical duration of the collision at interstellar temperatures is of the order of 10^{-13} s, whereas the radiative lifetime τ_r for pure vibrational transitions is of the order of 10^{-3} to 10^{-2} s. Thus, radiative association would occur only once every 10^{10} collisions.

There are circumstances, however, under which radiative association can occur more efficiently. In the most favorable case (Figure 11.27b), an attractive excited electronic state is accessible, so that the complex can be stabilized by a strong electronic transition. The lifetime for a dipole-allowed transition may be as short as 10^{-8} s, so that the process becomes 5-6 orders of magnitude more efficient. The important radiative association reaction

$$C^+ + H_2 \quad \rightarrow \quad CH_2^+ + h\nu \qquad (11.43)$$

can proceed through an excited electronic state, and is therefore rapid enough to initiate the formation of carbon-bearing molecules in interstellar clouds.

A related process, sometimes called "inverse predissociation", is illustrated in Figure

11.27c. Here the initial approach is along the ground state potential curve, but a radiationless transition can occur to an excited electronic state. This state has bound levels lying below the ground state dissociation energy, but correlates with excited species and is thus not directly accessible. The subsequent stabilization through the electronic transition is again rapid.

The efficiency can also be enhanced by an increase in the collision time and the time for redissociation into products (τ_d). One possibility is illustrated in Figure 11.23d, where metastable levels exist behind a potential barrier in which the molecules can be trapped. This process can be regarded as "inverse vibrational predissociation". The increase in τ_d is determined by the tunneling rate through the barrier, which depends sensitively on the height of the barrier and the collision energy.

For larger molecules, the duration of the collision process is also increased because the collision energy can be distributed over a larger number of vibrational degrees of freedom of the intermediate complex $(XY)^*$. Thus, the statistical probability that the energy is located in the mode leading to redissociation is smaller, and the molecule has more time to emit a photon.

b) Rate coefficients

The first semi-classical description of radiative association was given by Bates (1951, MNRAS **111**, 303). Quantum mechanical formulations have been developed for diatomic molecules. For polyatomic systems, statistical aproximations to the quantum mechanical theories are generally used to calculate the rate coefficients for the formation of the intermediate complex $(XY)^*$ and its redistribution into reactants. The calculations also need estimates of the radiative lifetime of the complex. These rate coefficients are sensitive to the nature of the reactants, and to the energy level structure and radiative transition probabilities of the collision complex, all of which are usually not well known. The resulting theoretical rate coefficients are therefore often uncertain by 1-2 orders of magnitude, and are modified with great regularity as new experimental or theoretical data become available.

Most theoretical studies of radiative association have considered only one potential energy surface (see Figures 11.27a and d). It has recently been argued that processes involving excited electronic states, such as depicted in Figures 11.27b and c, may be more common in the radiative association of poyatomic species than thought previously. Because the stabilization can occur through a rapid electronic transition in that case, the theoretical rates are expected to be larger than thought before. The lack of detailed information on the potential surfaces for the complexes, and on the radiative transition probabilities connecting them with the ground state, prevents at present an accurate determination of the rates for these processes.

Experimental data on radiative association at low temperatures are unfortunately still very limited. Because the process is so slow, three-body associations

$$X + Y + M \;\; \rightleftharpoons \;\; XY^* + M \;\; \rightarrow \;\; XY + M \tag{11.44}$$
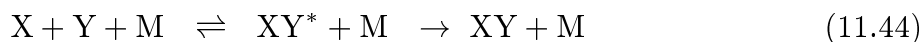
occur much more rapidly. Such experiments have been used to extract information on the lifetime of the collision complex τ_d, which, together with estimates of its radiative lifetime, allows a semi-empirical estimate of the two-body radiative association rate coefficient.

Only one astrophysically important two-body radiative association rate coefficient has been measured directly in the laboratory (Barlow, Dunn and Schauer 1984, *Phys. Rev. Letters.* **52**, 902):

$$CH_3^+ + H_2 \to CH_5^+ + h\nu. \tag{11.45}$$

The experimental rate coefficient of 1.8×10^{-13} cm^{3}s^{-1} at 13 K is an order of magnitude larger than the theoretical estimates at 10 K of $(1\text{-}3) \times 10^{-14}$ cm^{3}s^{-1}. The discrepancy is actually worse than it appears, because the experiments were performed using a normal hydrogen mixture with o-H$_2$/p-H$_2$=3/1, whereas the theoretical values pertain to *para*-hydrogen only. Since radiative association with o-H$_2$ is predicted to be slower than that with p-H$_2$, the experimental rate with p-H$_2$ is expected to be larger than the value mentioned above by a factor of four. However, additional experiments by Gerlich and Kaefer (1989, *Ap. J.* **347**, 849) suggest rate coefficients that are significantly lower, about 6×10^{-15} cm^{3}s^{-1} at 80K, and they also do not show a large sensitivity to the *ortho/para* ratio of H$_2$.

In summary, radiative association may be a relatively efficient process for the formation of the more complex molecules in interstellar clouds, but it is usually negligible for small molecules, except in special cases such as reaction (11.43). The process will be most efficient at low temperatures where the duration of the collision is longest. The rate coefficients decrease with increasing temperature as T^{-m}, where m lies in the range 0.5-2.5.

Ref: D.R.Bates and E.Herbst, in 'Rate coefficients in Astrochemistry.'

6. Three-Body Formation

a) Formation of grain surfaces

The only other process that can form molecular bonds in interstellar clouds occurs on the surfaces of the grains that are present in the cloud. Here the grain acts as a third body, which can absorb (part of) the energy that is liberated upon formation of the molecule. In interstellar clouds, the densities are too low for 3-body processes to occur in the gas-phase, but in planetary atmospheres where $n > 10^{12}$ cm^{-3}, these processes dominate the formation of the molecules.

In the interstellar process, the atoms (or smaller units) collide with a grain, stick to the cold surface, migrate from site to site, and form an adsorbed molecule, which eventually evaporates from the surface. The dominant molecule in interstellar clouds, H$_2$, is thought to be formed by this mechanism. Radiative association for this homonuclear molecule is in first order forbidden, and is thus much too slow to account for its large abundance.

The formation rate is determined by the frequency of collisions between the atoms and the grains, the sticking probability y_s, the probability y_r that the molecule formation occurs, and the probability for desorption from the surface y_d. The rate for the reaction of X with a grain g leading to the formation of XY

$$X + Y : g \to XY + g \tag{11.46}$$

can thus be written

$$r_f = n(X)n(g)\pi a^2 v_X y_s y_r y_d \quad [\text{cm}^{-3}\text{s}^{-1}] \tag{11.47}$$

where πa^2 is the mean cross section of the grains, v_x is the mean thermal speed of X, and y_s incorporates the number of species Y already on the grain surface and the likelyhood that a newly arrived X will encounter one. Extinction measurements suggest

$$\pi a^2 n(g) \approx 10^{-21} n_{\mathrm{H}} \qquad (11.48)$$

where $n_{\mathrm{H}} = n(\mathrm{H}) + 2n(\mathrm{H}_2)$, so that

$$r_f \approx 3 \times 10^{-18} T^{1/2} n_{\mathrm{H}} n(\mathrm{X}) y_s y_r y_d \ \ [\mathrm{cm}^{-3}\mathrm{s}^{-1}] \qquad (11.49)$$

for a typical atom X=C, O, N. The sticking probabilities, the nature and efficiency of surface reactions, and the desorption mechanisms of various species are still highly uncertain, so that the overall formation rates r_f are uncertain by orders of magnitude. The only exception is the formation rate of H_2, for which all three factors are believed to be close to unity. It is uncertain, however, how the energy liberated upon formation of the molecule is distributed between the grain and the translational and internal degrees of freedom of the newly-formed molecule.
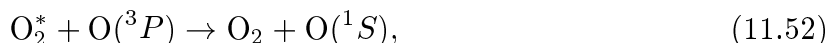
Ref: Watson and Salpeter 1972, Ap. J. **174**, 321; **175**, 659.
Allen and Robinson 1977, Ap. J. **212**, 396.
Tielens and Allamandola 1987, in 'Interstellar Processes'.

b) Example: the green light of the night sky

As we have seen, the $\mathrm{O}(^1\mathrm{S}) \to \mathrm{O}(^1\mathrm{D})$ green line at $\lambda 5577$Å is a prominent feature in the night sky. Although at high altitudes (for example the ionospheric F layer) the line results mostly from dissociative recombination of O_2^+ or reactions of N with O_2^+, it is produced by a chemical reaction in the lower layers involving 3 bodies. Chapman proposed in 1931 that the process results from the three-body reaction

$$\mathrm{O} + \mathrm{O} + \mathrm{O} \ \ \to \ \ \mathrm{O}_2 + \mathrm{O}(^1S) \qquad (11.50)$$
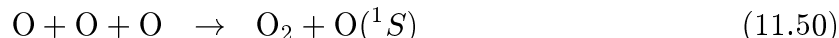
in which the O atom is produced in the excited ^{1}S state. Although estimates of the rate for reaction (11.50) proved difficult, this so-called Chapman mechanism remained accepted for more than 30 years. In 1961, however, Barth put forward a two-step process:

$$\mathrm{O} + \mathrm{O} + \mathrm{M} \ \ \to \ \ \mathrm{O}_2^* + \mathrm{M} \qquad (11.51)$$

$$\mathrm{O}_2^* + \mathrm{O}(^3P) \to \mathrm{O}_2 + \mathrm{O}(^1S), \qquad (11.52)$$

but tests of this mechanism were also plagued by the absence of reliable rate coefficients, especially for reaction (11.52).

The issue of the Barth vs. Chapman mechanism was not resolved until the early 1980's, when a combination of observations and laboratory experiments became available. A crucial piece of information came from the observation that the $\lambda 5577$Å green line is very weak in the Venusian nightglow. This virtually eliminated the Chapman mechanism, because the temperature dependence consistent with the Earth's atmosphere data would produce a too strong line in the colder atmosphere of Venus. In addition, efforts continued

to identify the O_2^* excited state in the Barth mechanism. Energetics indicate that only the O_2 c $^1\Sigma_u$, A$'$ $^3\Delta_u$ or A $^3\Sigma_u^+$ states are possible at 4.05, 4.24 and 4.34 eV, respectively. Both the a $^3\Sigma_u^+$ →X $^3\Sigma_g^+$, the A$'$ $^3\Delta_u$−a $^1\Delta_g$ and the c $^1\Sigma_u^-$−X $^1\Sigma_g^+$ forbidden bands have been seen in the terrestrial night glow. The same bands have also been seen on of Venus, except that in that case only the $v'=0$ level of the A, A$'$ and c states is observed. For the A $^3\Sigma_u^+$ $v' = 0$ and A $^3\Delta_u$ $v' = 0$ levels, reaction (11.52) is still exothermic, but for the c $^1\Sigma_u^-$ $-v' = 0$ state, it is endothermic. Since the $\lambda5577$Å line is prominent in the terrestrial atmosphere where $v' > 0$ levels are populated, but not in the colder atmosphere of Venus, this suggests that the c $^1\Sigma_u^-$ state is the intermediate O_2^* state in the Barth mechanism.

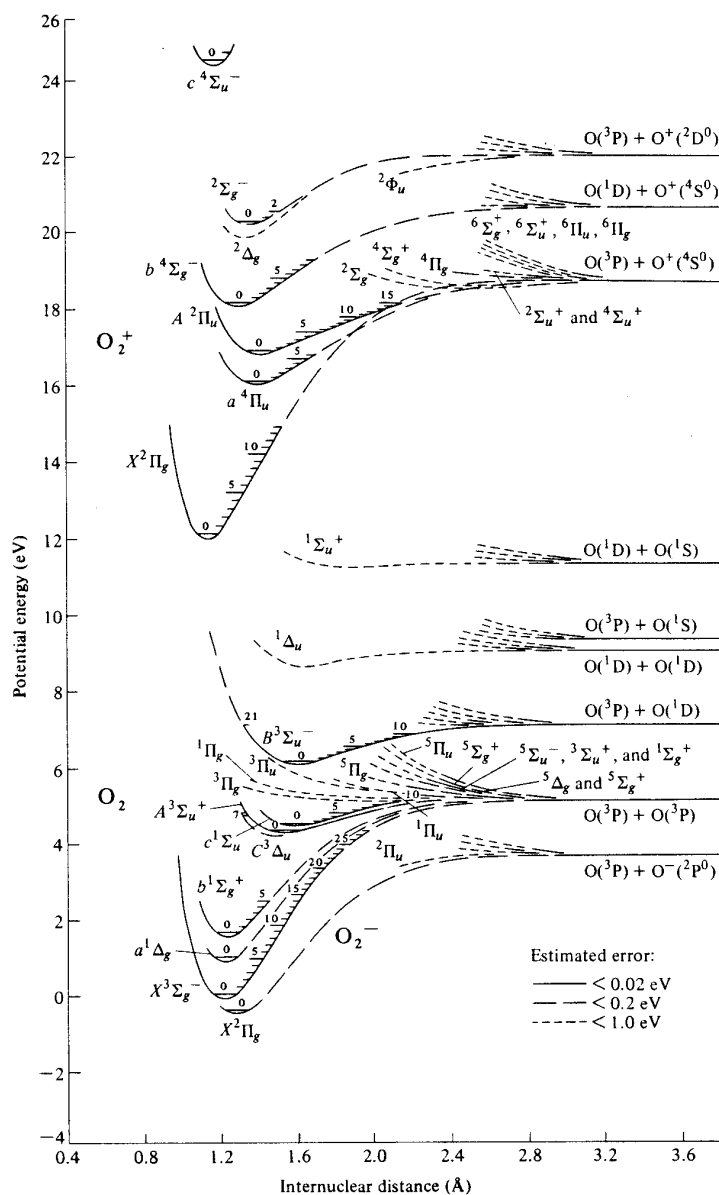**Ref**: D. R. Bates 1981, Planet. Space Science **29**, 1061.

Figure 11.28– Potential energy diagram for O_2 (compiled by F.R. Gilmore).